THE DESIGN AND CONSTRUCTION OF AN INPILE IRRADIATION SAMPLE AND ASSOCIATED INSTRUMENTATION FOR THE SIMULATION OF VERY HIGH FLUX NEUTRON IRRADIATION EFFECTS ON SEMI-CONDUCTOR MATERIAL

by

Timothy Peter Hulick

THE DESIGN AND CONSTRUCTION OF AN IN-PILE IRRADIATION SAMPLE AND ASSOCIATED INSTRUMENTATION FOR THE SIMULATION OF VERY HIGH FLUX NEUTRON IRRADIATION EFFECTS ON SEMI-CONDUCTOR MATERIAL

by

TIMOTHY PETER HULICK

B.S., United States Naval Academy
(1964)

SUBMITTED IN PARTIAL FULFILLMENT OF THE
REQUIREMENTS FOR THE DEGREES OF
NAVAL ENGINEER AND MASTER OF
SCIENCE, NUCLEAR ENGINEERING
at the
MASSACHUSETTS INSTITUTE OF TECHNOLOGY

May 23, 1969

THE DESIGN AND CONSTRUCTION OF AN IN-PILE IRRADIATION SAMPLE AND ASSOCIATED INSTRUMENTATION FOR THE SIMULATION OF VERY HIGH FLUX NEUTRON IRRADIATION EFFECTS ON SEMI-CONDUCTOR MATERIAL

by

Timothy Peter Hulick

Submitted to the Department of Naval Architecture and Marine Engineering and to the Department of Nuclear Engineering on May 23, 1969, in partial fulfillment of the requirement for the degrees of Naval Engineer and Master of Science, Nuclear Engineering.

Abstract

It is known that defects are produced in a crystalline solid when the crystal is exposed to bombardment by energetic neutrons. Semi-conductor material is especially sensitive to irradiation when used as a semi-conductor device since minute physical changes in a semi-conductor can cause large electrical changes. As nuclear reactors of higher fast neutron fluxes are developed (10^{16}n/cm^2/sec and above), first hand experiments in these flux ranges on irradiational behavior of semi-conductor material will be possible. The effects of very high neutron flux bombardment on semi-conductor material at room temperature can be simulated by irradiation at the liquid helium temperature and annealing at room temperature.

The time of irradiation at 4.2°K, the transit time in heating the semi-conductor material to room temperature or some other desired elevated temperature, the length of time that the specimen is held at the annealing temperature and the length of time involved in cooling the sample back down to 4.2°K must all be controlled according to the experimenter's specifications. Also, some property of the sample must be constantly monitored so that the appropriate changes in the chosen property can be observed. The physical property most easily measured remotely is electrical resistance or resistivity.

The design of a satisfactory semi-conductor holder, a sample heater, and ohmic contacts for continued in-pile usage that can withstand hundreds of repeated heating-cooling cycles from 4.2°K to 270°K and the associated instrumentation necessary to provide controlled heating and cooling of the sample and continous monitoring of resistance of the semi-conductor sample are the accomplishments of this thesis.

Thesis Supervisor: Thomas O. Ziebold
Title: Associate Professor of Nuclear Engineering

Thesis Reader: Jerome H. Milgrim
Title: Assistant Professor of Naval Architecture

ACKNOWLEDGEMENTS

The author wishes to express his gratitude to Professor Thomas O. Ziebold, his thesis supervisor, for his original thoughts concerning the theory and its development, suggestions on how to attack the problem, aid in data interpretation, and considerable help in organizing the writing of this thesis. Special thanks go to Professor Jerome H. Milgrim for accepting the role of thesis reader.

The author also wishes to acknowledge Dr. Manfred Lichtensteiger for his help in obtaining germanium and his many helpful hints on how to machine the material. Thanks go to John Dressler for disclosing to the author his method for depositing stannous-oxide films and for the use of his equipment for doing this. Thanks also to Fred Wilson for the use of his miniature sandblaster and to Robert Cavaleer and Phil Thullen of the Cryogenic Engineering Laboratory for their most helpful hints on using liquid helium. Gratitude to Ralph Burgess is also expressed for his consultation on circuitry and for the use of his silver epoxies.

A special thanks to Dr. Thomas Quinn of the Office of Naval Research for his help in financing this thesis and to the author's short order typist, Mrs. Pat Sedgwick, who worked untiringly into the advanced hours of darkness for many evenings.

More than gratitude is in order to the author's wife, Jo Anne, who has born him four children and in her patience has temporarily assumed the role of "father" and "thesis widow" during the interim necessary to complete this thesis.

TABLE OF CONTENTS

LIST OF SYMBOLS

i -- instantaneous current

I_b -- transistor base current

I_c -- transistor collector current

I_{RMS} -- root-mean-square value of current

k_1 -- rate constant (for introducing crystalline defects)

k_2 -- rate constant (for removal of crystalline defects)

k_3 -- rate constant (for introducing crystalline di-vacancies)

N -- total number of recovery cycles

n -- a particular recovery cycle between 1 and N

p -- concentration of crystalline defects

P -- heater power

T -- temperature

T_1 -- turn-off time of SCR

t -- time

V -- stannous-oxide film voltage

v_1 -- number of crystalline vacancies

v_2 -- number of crystalline di-vacancies

V_s -- voltage measured by the oscilloscope for ultimate determination of germanium resistance

ϕ -- actual neutron flux

ϕ' -- simulated neutron flux

δt_i -- low temperature exposure time

δt_r -- high temperature recovery time

β -- ratio of I_c to I_b

CHAPTER I

INTRODUCTION AND THEORY

1.1 Introduction and Problem Statement

Over the history of radiation studies it has commonly been assumed, explicitly or implicitly, that the observable changes in the properties of materials caused by neutron bombardment depend only on the total exposure, not the radiation flux. This supposition has been justified experimentally, but it is suggested that this is the case only because available radiation sources are limited in their intensity. However, in the case of long term devices such as structural materials and electrical components, namely semi-conductors, located in or near fast reactors or fusion power devices where neutron radiation is two orders of magnitude more intense than any test facility can presently provide, it is necessary to reexamine the role of the rate of introducing defects and not simply total exposure.

A number of authors have suggested that neutron flux should be an important variable in radiation effects studies. Dienes and Damask[1] and Brinkman and Wiedersich[2] discuss the influence of radiation on diffusion in solids and show that the enchancement of diffusion-controlled processes is directly proportional to the magnitude of the flux or its square root depending upon the recovery kinetics assumed (linear or bimolecular, respectively). Hesketh[3] and Ross-Ross[4] considering the effect of flux on in-reactor creep of metals, suggest that the rate of creep or stress relaxation will be directly proportional to rate of damage introduction. Recently, Lewis[5] has emphasized the need for testing materials in the very high fluxes which

are expected in large fast breeder reactors. There is an obvious need for more extensive consideration in high neutron flux effects on metallic crystals when it is realized that the neutron flux from a 100 kiloton fission explosion is about $4 \times 10^{19} n/cm^2/sec$,[6] at a distance of 500 yards. This flux is proportional to the payload tonnage of the bomb, and exists but for 10^{-6} second.

Intuitively, one feels that dynamic processes in metals (diffusion-controlled phase reactions, void growth phenomena, creep, etc.) must in some way depend on the rate of damage. That strong dependencies have not been seen to date probably indicates that the radiation-induced kinetics are additive to thermally-induced kinetics and hence are not observed until flux levels exceed those available today. With a valid simulation of high flux radiation, i.e., suppression of thermally-induced kinetics, the effects of flux on radiation damage should be enhanced to the level of observability.

The accomplishment of this thesis is the derivation of a valid very high flux simulation technique such that the effects of this high neutron flux can be observed experimentally by exposing a germanium sample to much lower more attainable neutron fluxes such as that available in the MIT Reactor, i.e., 2×10^{13} neutrons/cm^2/sec. Germanium has been chosen as the sample material to be tested because small changes in crystalline structure (doping, point defects, etc.) result in large changes in electrical parameters which can readily be observed. The germanium can therefore, be representative of other metallic crystals and is also directly representative of semi-conductor behavior under neutron bombardment.

The following theoretical development is a result of many long discussions with T. O. Ziebold* on the feasibility of such a simulation.

1.2 Assumptions and Theoretical Development

The kinetics of generation and rearrangement or removal of crystalline defects resulting from radiation bombardment are complex, and they depend on what is meant by a "defect." For purposes of illustrating the principle of simulating a high flux environment, however, consider a simple case, but one which may apply, at least to a first approximation, to certain real processes. Assume that the concentration of defects, p, changes with time as given by

$$\frac{dp}{dt} = k_1\phi - k_2 p \qquad (1)$$

This indicates that the rate of introducing defects is proportional to the neutron flux, ϕ, and that these defects are removed by a first-order kinetic process with appropriate rate constants k_1 and k_2. The solution to this equation (for $p = 0$ at $t = 0$) is, of course,

$$p = (k_1\phi/k_2)(1 - e^{-k_2 t}) \qquad (2)$$

If it is assumed that k_1 is not dependent on temperature and that k_2 is not dependent on neutron flux (the validity of which is discussed later), the simulation of a high and experimentally unattainable flux is achieved in the following manner. An irradiation cycle of alternate periods of exposure at a sufficiently low temperature at which new

---

*Associate Professor of Nuclear Engineering, Massachusetts Institute of Technology

defects will be frozen in as they are generated, followed by short recovery periods at some higher temperature during which the defects are allowed to partially relax will be used. The number of defects introduced by each low temperature exposure of period δt_i is $k_1 \phi \delta t_i$ and the number of defects remaining after the Nth recovery cycle will be

$$p_N = (k_1 \phi \delta t_i + p_{N-1}) e^{-k_2 \delta t_r}$$

$$= k_1 \phi \delta t_i \sum_{n=1}^{N} e^{-n k_2 \delta t_r}$$

$$p_N = (k_1 \phi / k_2)(\delta t_i / \delta t_r)(1 - e^{-N k_2 \delta t_r}) \left[(k_2 \delta t_r) / (e^{k_2 \delta t_r} - 1) \right] \qquad (3)$$

The factor in brackets is an indication of the error incurred unless the recovery periods are short. For sufficiently short intervals, i.e., $k_2 \delta t_r << 1$, the expression reduces to

$$p_N = (k_1 \phi / k_2)(\delta t_i / \delta t_r)(1 - e^{-N k_2 \delta t_r}) \qquad (4)$$

which may be compared to equation (2). Equation (4) indicates that a high flux, ϕ', may be simulated using an available flux, ϕ, simply by scaling the cyclic periods so that the irradiation interval δt_i is greater than the recovery interval δt_r by a factor of ϕ'/ϕ.

It must be remembered that the kinetic processes indicated by equation (1), i.e. a constant introduction of defects and a first-order

removal, may be too simple of a description for most real processes although the analysis by Dienes and Damask indicates that first-order kinetics are appropriate for short range diffusion controlled processes. Even if the net change in elementary point defects (vacancies and interstitials) is considered, the process is probably second-order (bimolecular) or a combination of the two except at very low temperatures. In this case the cyclic time scaling factor would be the square root of the ratio of simulated to actual flux. If the next simplest defect is considered, i.e., a di-vacancy, a process can be imagined characterized by

$$\frac{d\,v_2}{dt} = k_1\phi + k_3\left[v_1\right]^2 - k_2\left[v_2\right] \qquad (5)$$

where the first term on the right expresses the direct introduction of di-vacancies by bombardment, the second term recognizes the introduction of a di-vacancy from the joining of two single vacancies, and the third term accounts for the removal of di-vacancies by some process which depends solely on their concentration. Considering more complex defects suggests many more possible interactions which may embrace various combinations of sequential and parallel kinetics.

At this point it must be realized that defect concentrations can only be measured indirectly. Thus, what is meant by a "radiation defect" depends on the physical, chemical or mechanical property being measured. It is generally supposed that the number of elementary point defects (vacancies and interstitials) can be quantized by changes in electrical reisitivity or resistance, although, even here there is a

question about the unit change in resistivity of a point defect by itself or when associated with other defects such as impurities, dislocation jogs, etc. When mechanical properties are the properties to be observed, it becomes difficult to identify which defects are the ones affecting the property, let alone to establish what specific effect is noticed on that property. Nevertheless, if the change in a particular property can be validly separated from the thermal redistribution of these defects to a thermodynamically stable configuration by the direct introduction of defects by bombardment, then the simulation technique described above will at least indicate the right direction toward establishing damage rate, or flux dependence, of whatever processes may be occurring.

As estimated by many approaches, well known by now, the time duration of a displacement cascade is on the order of 10^{-13} seconds. Including in this event the immediate athermal relaxation of mechanically unstable defects, the entire introduction of new defects occurs in a time of about 10^{-12} seconds after the initial primary knockon is created by an incident neutron. Conversely, thermal recovery processes are characterized by time constants measured in minutes or hours. Typically, the mean residence time for a vacancy on a lattice site in iron at 500°C, for example, is on the order of 10^{-5} seconds so that even short range thermally activated interactions must be on a time scale much slower than that which characterizes a displacement cascade.

The above technique, therefore, seems to be a valid simulation of irradiation exposures in which, by scaling the alternate irradiation

and recovery cycles, the investigation of the phenomena of radiation damage for neutron fluxes which are far above those available in experimental facilities, is possible.

According to the above discussion it will be possible to simulate a flux of 10^{16} neutrons/cm^2/second by actual exposure to a flux of 2×10^{13} neutrons/cm^2/second with alternate low temperature periods and high temperature (annealing) periods of 5000 seconds and 10 seconds, respectively. Since these times differ by a factor of 500, insignificant radiation damage will result during the annealing time. The annealing kinetics indicated by "k_2p" in equation (1) are therefore not a function of ϕ, i.e., $k_2 \neq f(\phi)$. Likewise, since virtually no annealing takes place when ϕ is significant, (during the 5000 second irradiation time), $k_1 \neq f(T)$, the annealing temperature, because the irradiation occurs at a temperature below that at which annealing takes place, i.e. $4.2^{\circ}K$.

It must be remembered that the experiment proposed deals with noninfinitesimally short lengths of both irradiation and recovery times and therefore deviates from the solution to the integral form of equations (3) and (4). At best the simulation of high flux neutron effects on crystalline solids, particularly semi-conductors, is an approximation that cannot converge on the integral limit, but does at least propose a valid approximation to that limit.

CHAPTER II

THE IRRADIATION SPECIMEN ASSEMBLY

2.1 Selection of a Suitable Irradiation Specimen Material

The selection of materials necessary to comprise an irradiation sample was based on the requirements that the sample assembly must be capable of

1) remaining physically intact under high neutron exposure,
2) being frozen to the temperature of liquid helium (4.2°K) and heated directly or indirectly to some elevated temperature in a few hundred milliseconds and then refrozen just as repidly without the threat of thermal shock,
3) temperature recycling several hundred times and remaining free of plastic strain,
4) being designed into a small package with the largest dimension less than 3/4 inch,
5) being very light weight, and
6) being made as simple as possible for instrumentation purposes.

This was a design problem that proved to be quite difficult but not impossible to solve.

The irradiation specimen is to be inserted into the vertical section of the closed loop liquid helium irradiation facility presently being installed in the center of the MIT Reactor core for the purpose of carrying out irradiation experiments such as the one proposed here. The inside diameter of the cryostat chamber comprising the vertical section of interest in 3/4 inch. Access to the center of the core is available at the top of the vertical channel. Figure 1 is an illustration[7]

of the section of the liquid helium loop that is to house the irradiation sample. The inside diameter of the helium tube places the restriction of 3/4 inch as the maximum dimension of the sample.

Before the specific design of a sample assembly could be considered, it was necessary to decide which physical property of the sample was to be measured and what material was to be used as the actual specimen itself. From the first concept of the experiment, germanium was the primary material considered and soon to be the only material seriously considered for several reasons: electrical resistance or resistivity is easily measured and is a sensitive indication as to the crystalline condition of the metal, i.e., doping, residual stresses, point defects, etc. Futhermore, in semi-conductors the resistivity changes markedly for minute crystalline changes, and the use of germanium would represent semi-conductor behavior directly as a function of neutron flux and would represent other metals indirectly. Silicon could offer the same advantages, however germanium proved to be more readily available.

2.2 Design of the Germanium Heater

Because of the short annealing time (10 seconds or less) desired, it would be impractical to remove the germanium specimen from the liquid helium flow each time that the sample was to be annealed. The use of an in-pile, in-liquid helium heater is pertinent to the success of this experiment.

Heating the germanium directly by passing direct current through it and monitoring resistance by an alternating current (say 10 KHz. since this frequency and direct current are easily separable) would naturally make the specimen simple and easy to construct, but at the same time

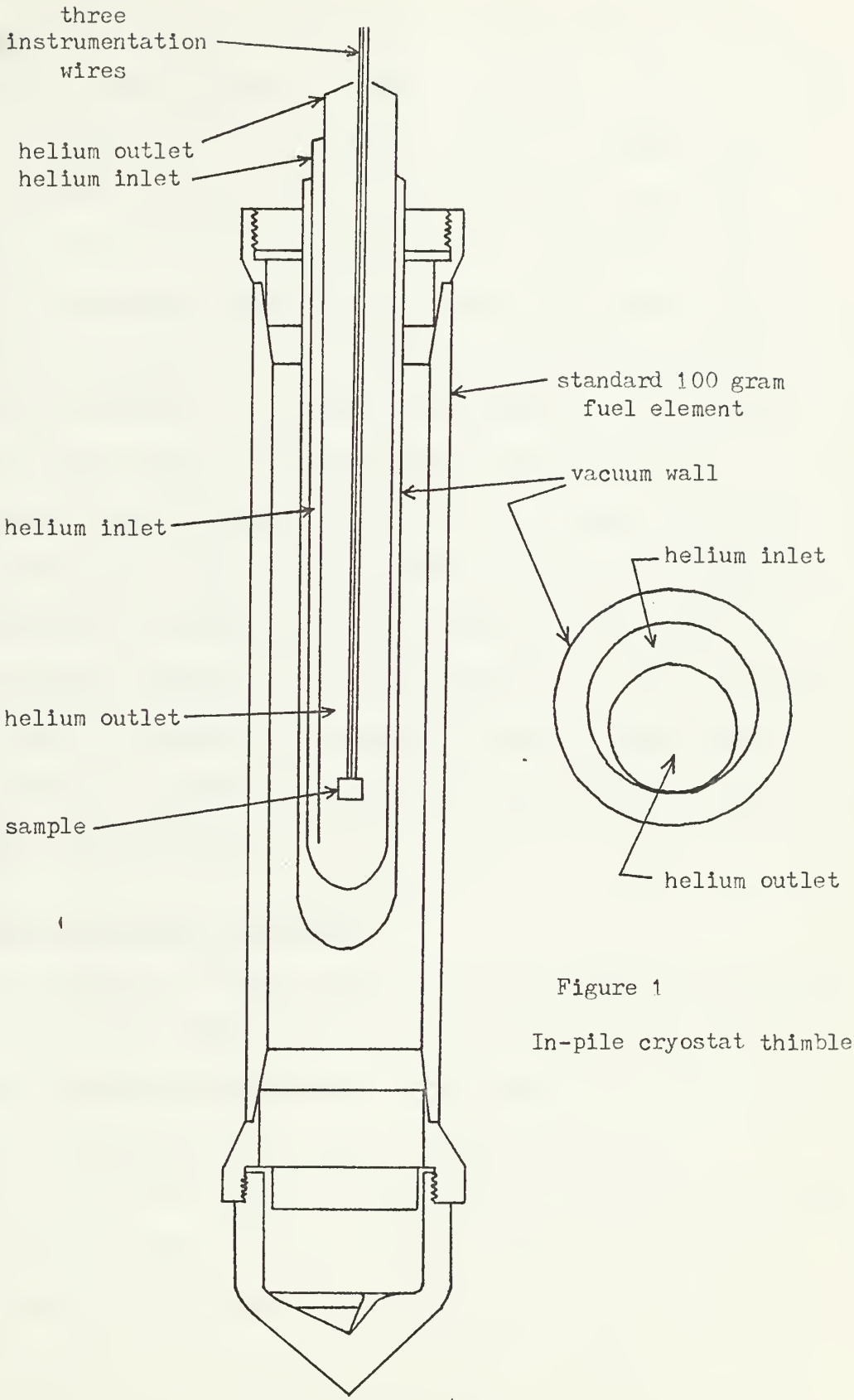

Figure 1

In-pile cryostat thimble

proved to be impractical since the resistance of all the intrinsicly doped germanium wafers obtained increases from about 12 kilohms at 270°K to about 500 kilohms at 4.2°K. Extremely high d.c. voltages would be required to generate any heat at all in the germanium at this high resistance. At this point it was realized that some heater element other than the germanium itself with resistivity only a weak function of temperature or at least one with a positive temperature coefficient of resistivity would have to be used. Additionally, it is desirable to make the heater separate from the sample so that the heater resistance and power requirements will be the same when a variety of specimen materials is tested. This restriction invites new problems such as discovering a material which is an electrical insulator and yet a good thermal conductor at cryogenic temperatures. The electrical insulator would be necessary to insulate the electric heater from the germanium and still provide a low resistance heat conduction path to the germanium from the heater.

2.3 Selecting a Suitable Dielectric

Any of the forms of silica could serve as an electrical dielectric, but quartz has a much higher value of thermal conductivity at cryogenic temperatures than plain silica glass. (see Figure 2)[8]. In fact, prior to any neutron irradiation, quartz has a thermal conductivity approximately 10^4 times as great as silica glass, but after irradiation, it is apparent from Figure 2 that the thermal conductivity of quartz approaches that of silica glass since neutron radiation disrupts the crystalline material until finally with extensive exposure, all traces of crystallinity are lost. For the irradiation and in-pile annealing

Fig. 2

Thermal Conductivity Vs, Temperature
For Quartz
As a Function of Neutron Irradiation

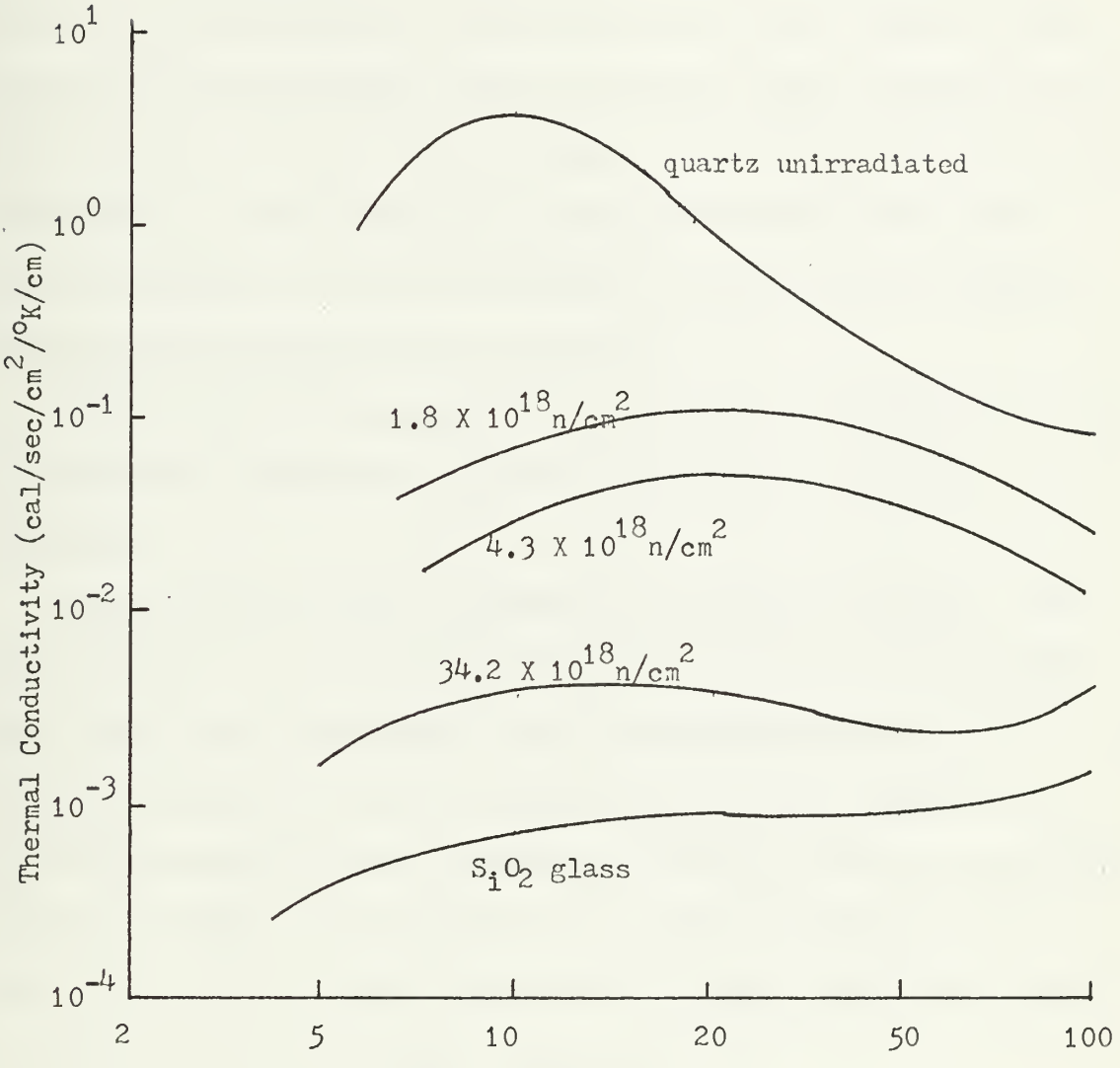

period used in this experiment, (5010 seconds/cycle) approximately 500 heating-cooling cycles under an actual flux of 2 X 10^{13}n/cm^2/sec could be performed before the crystalline structure of the quartz would be destroyed. This provides a total exposure time of 696 hours or about 29 days that the experiment could be continuing before the quartz would turn to glass. However, if the germanium could still be heated to room temperature at a sufficiently high warm-up rate after 29 days, then there is no reason to stop the experiment because the thermal conductivity of the quartz has greatly decreased.

After examining the properties of quartz it was decided to use it as the required electrical insulator between the heater and the germanium.

Quartz wafers are quite inexpensive and readily available. The source of pre-cut quartz wafers used in this experiment was discarded surplus type FT-243 piezoelectric radio transmitting crystals. The typical dimensions of a quartz crystal from the FT-243 holder is one centimeter square at various thicknesses depending upon the oscillating frequency intended. The crystalline orientation of the wafers in not known, but since the thermal conductivity of quartz varies only slightly for different cuts, this is not important.

Since piezoelectric crystals are etched in hydrofluoric acid, the surfaces must be polished on a polishing wheel with 0.3μm alumina grit and distilled water. The mirror finish provides for greater surface contact to the germanium wafer so that the thermal conductance at the germanium-quartz interface is maximized.

2.4 Electric Heater Material

It was stated earlier in section 2.2 that it proved to be impossible to heat germanium directly by passing an electric current through it since the resistance of all the intrinsically doped specimens obtained (intrinsic germanium has a lower resistivity than any non-intrinsic germanium) is much too high at 4.2°K to allow heater voltages of practical magnitude to be used.

The germanium-quartz specimen allows a heater to be installed on the quartz face opposite the germanium. Aqua-dag was considered to be a possibility but soon discarded because it suffers permanent resistance changes upon heating. These resistance changes are on the order of thousands of ohms for temperature changes of several hundred degrees Fahrenheit. Change of resistance with temperature was measured for other heater possibilities and by far the most promising material was a stannous-oxide film on glass. A sample stannous-oxide film on a microscope slide with a specific resistance of 27 ohms per square* was tested for ruggedness and resistance changes as a function of temperature. These tests showed that the stannous-oxide film resistance changed from 27 ohms per square at 300°K to 30 ohms per square at 4.2°K. (a change of only 11%). In this respect, the stannous-oxide film was far superior

---

*Since resistance of a sheet of width w, length l, and thickness t is $R = \rho l/wt$, where ρ is the resistivity, then for a fixed thickness the resistance is the same for a square sheet ($l = w$), regardless of the size of the square. This is the reason for reporting the resistance of the films as "ohms per square".

to any other potential heater element. After further investigation the stannous-oxide film proved to be insoluble in both hot and cold water, liquid nitrogen or liquid helium and cannot be scratched significantly even with sandpaper. All efforts to remove it from the glass surface failed except for the fact that it can be etched by a combination of zinc dust and a 0.4 volume percent solution of hydrochloric acid. More extensive tests showed that it can withstand thermal shock at least as well as what is necessary to make it a successful heater for this experiment since preliminary testing proved that heating the glass, stannous-oxide combination in a liquid helium bath in a few hundred milliseconds from $4.2^{\circ}K$ to $270^{\circ}K$ caused no cracking of the slide or permanent resistance change of the stannous-oxide film. Furthermore, the total cross-section, σ_T, of tin is comparable to that of aluminum so that it will not become intolerably radioactive. In brief, the stannous-oxide film on glass is virtually indestructible.

The first attempt to deposit a stannous-oxide film on quartz proved to be successful. It was discovered that the film would adhere extremely well to anything it came in contact with except, of course, grease or dirt. Depositing a stannous-oxide film on quartz or glass is quite simple, but not a well known process. The following is a method describing the deposition procedure.

The below listed weight proportions are mixed in a glass beaker:

66% acetone

33% stannic-chloride pentahydrate

1% antimony trichloride

The latter two constituents will dissolve in the acetone with stirring. The mixture will take on a very slight bluish cloudiness when the stannic chloride pentahydrate and antimony trichloride are fully dissolved in the acetone.

After polishing, the quartz must be thoroughly washed with soap and water. It is essential to have the quartz face absolutely clean. It is then placed on a microscope slide and clamped down in some manner such as by a weight resting on one corner of the quartz. The slide, quartz, and weight are then placed in an oven and heated to 600°C. It is pertinent to obtaining a successful stannous-oxide film that the deposition surface be at a temperature of at least 600°C. It is appropriate to mention that quartz experiences a volumetric phase change[9] at 573°C and therefore one would expect the quartz-stannous-oxide interface to break-up upon cooling through this temperature since the stannous-oxide does not experience a similar phase change. In spite of this, it is not drastic enough to disrupt the bond between the quartz and stannous-oxide. An attempt to deposit the film on the quartz at a temperature below 573°C was unsuccessful so that a quartz temperature of 600°C is imperative. The film on quartz combination suffers no apparent damage by heating to 600°C. When the oven temperature of 600°C is reached, the oven door can be opened and the acetone mixture sprayed onto the quartz surface for a total of about thirty seconds or so by means of a Paasche H "3 in 1" airbrush under a pressure of about 20 psi dry-nitrogen gas. One would expect the acetone mixture to ignite upon hitting

the hot air inside the oven, but this is not the case since the nitrogen sufficiently masks the acetone mist. After spraying, the oven can be turned off and the door left open until a temperature is reached at which the quartz-stannous-oxide film can be handled. The resistance can be checked by touch-down probes onto the film surface and a volt-ohm meter (VOM). This however will not indicate the specific resistance obtained since contact would have to be made all across two opposite edges of the film for obtaining this parameter, but the point contacts available by means of VOM probes will at least indicate whether or not the film deposition is conductive or not. The film appears slightly bluish when good and frosty when bad. If a frosty film develops the quartz was most likely not yet up to the oven temperature of 600°C.

After experience in stannous-oxide film deposition is gained, one can estimate how long the spraying time must be in order to obtain a desired specific resistance, but only within about 50% of the expected value. This has been the author's impression of this technique. A guideline however, is that for a spraying time of thirty seconds, the specific resistance will be about 200 ohms per square.

In using this technique the following precautions should be noted: The airbrush must be cleaned in soap and water after spraying is completed since the acetone, stannic-chloride pentahydrate, antimony trichloride mixture is highly corrosive to metal. The mixture can be stored in a covered glass beaker for about eight days at room temperature after which time it will turn yellow. After this discoloration takes

place, it is no longer a stable mixture and tends to become explosive. It can be flushed down a drain with copious amounts of cold water or discarded by some other appropriate means.

2.5 Assembly of the Completed Irradiation Specimen

Figure 4 is a detailed illustration of the completed germanium, quartz, and stannous-oxide film wafer with the associated electrodes and hardware. Dimensions of the assembly are not shown since the purpose of this illustration is to show general construction and relative positions of each component.

Germanium resistance is measured between bolt positions, i.e., along the length of the germanium and not through the thickness. The cross-sectional area for conduction is therefore, the product of the width and thickness of the germanium. The conduction path for the heater film is the same.

The entire assembly is held together by means of two steel .0096 size bolts. The assembly bolt holes were drilled by means of a small hand-held pencil-point size sandblaster. Using this method instead of diamond point drills is much faster and reduces the chance of damage to the germanium or quartz. Approximately thirty seconds are required to drill a hole through the sandwich.

The bolt on the left is electrically common to one pole of the heater and one pole of the germanium. This is the common ground connection labeled "C" as shown schematically in Figure 3 below.

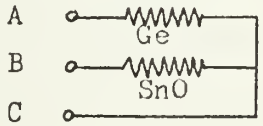

Fig.3

Good electrical contact is made to the germanium by means of a small square of .005 inch thick copper sheet mounted locally at the bolt hole as shown.

The bolt on the right in Figure 4 is not electrically common to the film and germanium. It must therefore be electrically insulated from one or the other. As shown, the bolt is electrically connected to the stannous-oxide film and insulated from the germanium by means of a glass bushing (short section of capillary tubing) which is long enough to extend from the bolt head to the nut. The ungrounded stannous-oxide film electrode and ungrounded germanium electrode each consist of a small square of .005 inch thick copper sheet and are electrically insulated from each other by means of a ceramic washer and the glass bushing.

Electrical contact to the film itself is made by two narrow strips of .005 inch thick copper sheets each mounted at and electrically in contact with a bolt head. These strips must be just long enough to reach the edges of the film. Unless these contacts span the full width of the film, heating will be concentrated within a narrow band symmetrical about a line drawn between the two bolt heads. It was also found necessary to use a small amount of conductive silver epoxy as a contour fitting filler between all copper strips and their respective areas of contact whether germanium or heater film. It should be emphasized that only a very small area between interfaces should be covered with the epoxy, since plastic strain of the germanium and film can result after temperature cycling. Evidence of this is apparent when the film or germanium resistance does not return to its previous value at a given temperature.

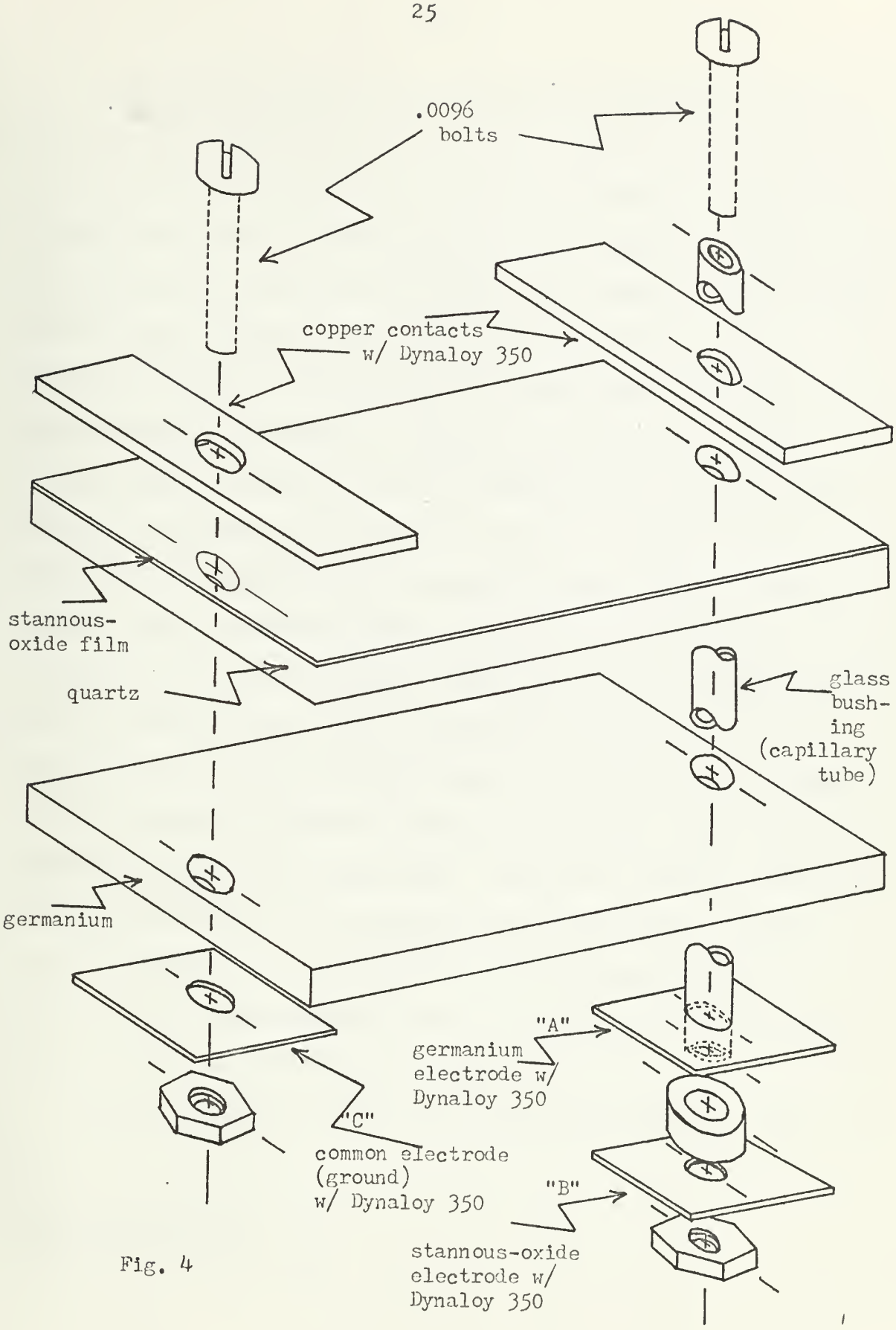
.0096
bolts
copper contacts
w/ Dynaloy 350
stannous-
oxide film
quartz
glass
bush-
ing
(capillary
tube)
germanium
"A"
germanium
electrode w/
Dynaloy 350
"C"
common electrode
(ground)
w/ Dynaloy 350
"B"
stannous-oxide
electrode w/
Dynaloy 350

Fig. 4

Since organic compounds are unacceptable in assemblies to be irradiated by neutrons, none of the common conductive epoxy resins can be used for the filler material. The only epoxy found to contain an insignificant amount of organic compounds after hardening is Dynaloy 350.* This epoxy consists of a mixture of fine silver pigment, acrylic resin, phenolic resin, toluene, xylene, and cellosolve acetate. After handening and baking at 200°F for about fifteen minutes, the only organic materials remaining are very small amounts of acrylic and phenolic resins. Dynaloy 350 is also solderable with lead-tin solder should it be necessary or convenient to do so. For these reasons, Dynaloy 350 was considered to be acceptable as the conductive filler. Once this epoxy is applied to the surfaces, the bolts should be tightened (but not overtightened). This epoxy becomes semi-hard after about two minutes in open air. It is fully hardened in about twelve hours after which time it should be baked at 200°F for fifteen minutes.

The sandwich can be made as small as the builder cares to make it. Thickness can be as thin as practical. Length and width are limited only by the bolt sizes used. Two completed samples are shown in Figures 14 and 15 in Chapter III. The dimensions of the smaller sample are 7mm X 5mm X 1mm thick excluding bolts and has a mass of 550 milligrams with bolts but less instrumentation leads.

A convenient means of holding two of the instrumentation leads

---

*Available from Dynaloy, Inc.
7 Great Meadow Lane
Hanover, New Jersey, 07936

together at the connections to the assembly is to use a "two wire glass bead" assembly found inside of any incandescent pilot bulb such as a #47 bulb. This, of course, is not absolutely necessary, but recommended. The wires from one side of the glass bead are soldered to the two ungrounded copper electrodes. Two of the three long instrumentation wires leading away from the assembly are soldered to the wires from the opposite side of the glass bead. The third instrumentation wire connects directly to the common or ground electrode on the wafer. All three wires are insulated from each other by small ceramic insulators for their entire length.

CHAPTER III

INSTRUMENTATION

3.1 Instrumentation Requirements

Even though the theoretical demands of this experiment require that the germanium, quartz, stannous-oxide specimen be heated as rapidly as possible from 4.2°K to the chosen elevated temperature, it was deemed wise to design the instrumentation to permit flexibility in the choice of elevated temperature, rate of heating, and length of time at the elevated and low temperatures. It was also the author's desire to design the apparatus with the maximum amount of automation feasible in order to accomplish the chosen rate of temperature rise, the elevated temperature and the length of time at this temperature for the convenience of future experimenters.

The device must be capable of holding accurately at the required heater voltage output necessary to bring the specimen to the desired predetermined annealing temperature rapidly without overshoot. A selectable rate of heater voltage increase would permit a fast or a slow increase in temperature rise of the irradiation sample to the selected annealing temperature. This requirement demands the utilization of some sort of negative feed-back system such that temperature rise is ceased when the desired temperature is reached. It was thought that since the resistance change with temperature of the stannous-oxide could be used as a resistance thermometer so that when the annealing temperature value of the film resistance was reached upon heating, it could be used to balance an audio frequency resistance bridge circuit. The balance of resistance would cause the bridge output voltage to go to zero, thereby

reducing the heater voltage increase rate to zero and hold the heater voltage to the value at which the rate increase circuit turned off. A circuit was designed to operate on this principle. Heater power was by direct current to the stannous-oxide film and a 10KHz audio signal was used to operate the null bridge circuit to measure temperature (i.e., resistance) of the heater. This principle worked well on dummy heaters such as aqua-dag resistors or carbon film resistors but did not work on the stannous-oxide film resistance because the resistance of the film does not change enough even over the wide temperature range involved. An 11% change in resistance in going from 4.2°K to 270°K was not enough to cause significant 10KHz bridge output voltage change to stop the rise in heater voltage. For this reason, this scheme was abandoned.

It was then decided to design the desired automatic heater system not to depend on the germanium or stannous-oxide film whatsoever. Being independent of the properties of the load would certainly be an asset that would ensure stability in respect to the automation circuits which in turn would result in stabilization of the annealing temperature.

It was thought that the circuit designed to cause the heater voltage to continuously rise could be turned off by the heater voltage when the latter matched that of a selected reference voltage internal to the instrument. The reference could be selected at will. When the heater voltage rise circuit was automatically turned off, the heater voltage would hold at the reference voltage selected and remain there until the experimenter turned it off at the end of the annealing phase of each cycle of the experiment.

Designing a circuit based on this principle seemed feasible. Since the rate of heater voltage rise circuit is independent of the heater level-off or hold circuit, the two could be adjusted independently.

3.2 Circuit Description

The circuit shown in Figure 1 was designed by the author to operate on the principle stated above. Each section of the circuit complete in a specific function will be analyzed.

The variable reference voltage power supply is comprised of T_1, D_1, D_2, C_1, C_2, C_3, R_1, R_2, R_3, R_5 and Q_1 as illustrated in Figure 2 below.

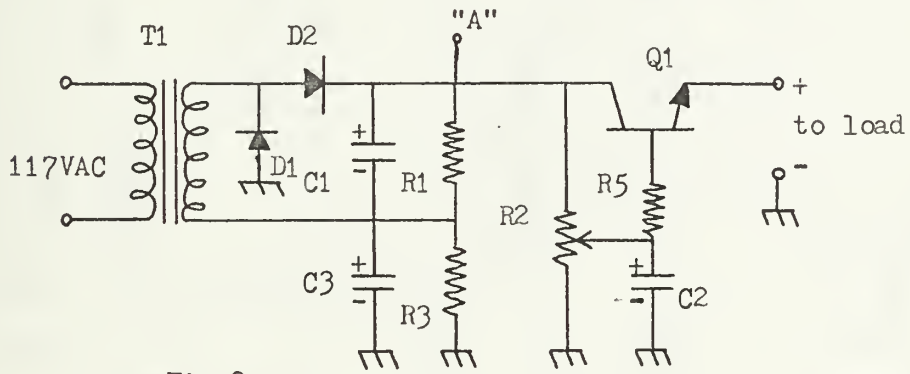

Fig.2

The purpose of T_1 is primarily to isolate the 117VAC line from the voltage reference supply. The secondary voltage of T_1 is 24VAC or 34 volts peak. D_1, D_2, C_1 and C_3 comprise a voltage doubler circuit by charging C_1 and C_3 in parallel but discharging them in series to a load. The d.c. voltage at point "A" with respect to ground is therefore 68 volts. C_1 and C_3 are each 500µf/35VDC electrolytic capacitors. This value of capacitance was arbitrarily chosen at this value to ensure d.c.

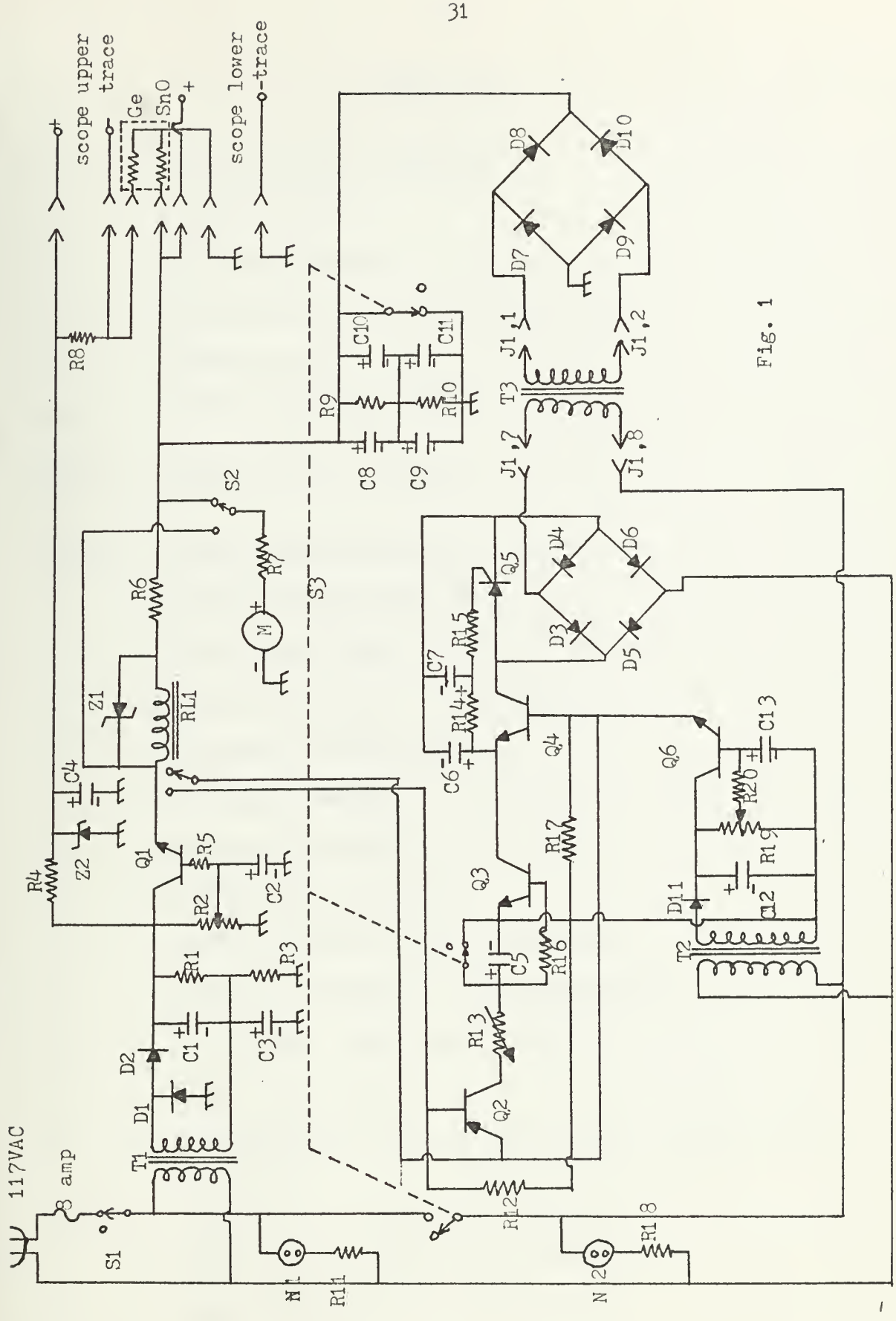
117VAC
amp
S1
T1
D1
D2
C1
C3
R1
R3
R2
C2
R4
Z2
Q1
R5
C4
Z1
RL1
R6
S2
R7
M
S3
R8
scope upper trace
Ge
SnO
+
scope lower -trace
R9
C10
C11
R10
C8
C9
D8
D10
D7
D9
J1,1
J1,2
T3
J1,7
J1,8
D4
D6
D3
D5
Q5
R15
C7
R14
C6
Q4
Q3
R17
C5
R16
R13
Q2
R12
R18
N 1
R11
N 2
Q6
C13
R20
R19
C12
D11
T2

Fig. 1

PARTS LIST

Q_1, Q_4 -- RCA 40491(SK3021) transistor

Q_2 -- 2N328A transistor

Q_3 -- RCA 40245 transistor

Q_5 -- RCA 2N3228 Silicon-controlled-rectifier

Q_6 -- 2N388 transistor

D_1, D_2 -- 1N2861A Silicon rectifier

D_3, D_4, D_5, D_6 -- 1N2862A Silicon rectifier

D_7, D_8, D_9, D_{10} -- 1N2864A Silicon rectifier

D_{11} -- 1N2858A Silicon rectifier

Z_1 -- 1N2977 Zener diode

Z_2 -- 1N747 Zener diode

N_1, N_2 -- Type NE-2 neon pilot bulb

S_1 -- SPST toggle switch

S_2 -- SPDT toggle switch

S_3 -- TPDT rotary wafer switch

T_1 -- 117VAC to 24VAC @ 1.2 amp. transformer

T_2 -- 117VAC to 12.6VAC @ 1.2 amp. transformer

T_3 -- Pri. 117VAC. Sec. refer to page 46

M -- 200μa. panel meter

RL_1 -- Phillips-Advance micro-miniature type NM Neomite relay (NM/1C/2000)

C_1, C_3 -- 500μf./35 volt electrolytic capacitor

C_2 -- 100μf./150 volt electrolytic capacitor

C_4 -- 200μf./6 volt electrolytic capacitor

C_5 -- 1000μf./25 volt electrolytic capacitor

C_6 -- 5μf./15 volt electrolytic capacitor

C_7 -- 50μf./15 volt electrolytic capacitor

C_8,C_9, C_{10},C_{11}- 1000μf./50 volt electrolytic capacitor

C_{12},C_{13}- 30μf./25 volt electrolytic capacitor

R_1,R_3, R_9,R_{10}, R_{11},R_{18}- 100 kilohm $\frac{1}{4}$ watt resistor

R_2 -- 10 kilohm $1\frac{1}{2}$ watt potentiometer

R_4 -- 3.9 kilohm 2 watt resistor

R_5 -- 27 ohm $\frac{1}{2}$ watt resistor

R_6 -- 1 kilohm 10 watt resistor

R_7,R_{16}-- 1 megohm $\frac{1}{2}$ watt resistor

R_8 -- 20 kilohm $\frac{1}{2}\%$ tolerance precision resistor

R_{12} -- 56 kilohm $\frac{1}{4}$ watt resistor

R_{13} -- 100 kilohm carbon potentiometer (linear taper)

R_{14} -- 470 ohm $\frac{1}{2}$ watt resistor

R_{15} -- 100 ohm $\frac{1}{4}$ watt resistor

R_{17} -- 10 kilohm $\frac{1}{4}$ watt resistor

R_{19} -- 2.5 kilohm subminiature screw driver adjust carbon potentiometer (IRC type X201R252B)

R_{20} -- 1 kilohm $\frac{1}{4}$ watt resistor

J_1 -- Octal socket pair. Pins 1,2,7 and 8 used only

with less than 1% ripple voltage at point "A" under a 200 milliampere load. 250μf (C_1 and C_3 in series) is a vast over design in this respect but these capacitors are physically small and no more expensive than capacitors of half their value, therefore, they were used. (In designing power supplies, an overestimation of filter capacitor size is an asset when charging time constants are not important providing the capacitors are physically not too large). R_1 and R_2 are equal in resistance and help to ensure that the 68 volts at point "A" is equally divided across C_1 and C_3. R_2, R_5, C_2 and Q_1 form a series type voltage regulator. It is a series type because the current path from collector to emitter through transistor Q_1 is in series with the ultimate load. The resistance of the collector to emitter current path is made variable by the choice of transistor Q_1 base current which can be selected by the slider position of R_2. When the base-emitter PN junction is biased in the forward direction by moving the slider of R_2 toward the collector end, the collector to emitter resistance is minimized, therefore most of the 68 volts appears across the ultimate load. If the slider of R_2 is shifted to the ground side the base-emitter junction of Q_1 is biased to zero, no base current will flow and the collector to emitter resistance approaches infinity (the transistor goes to cut-off). Consequently, the 68 volts appear entirely across the collector-emitter circuit and zero voltage across the load. In light of this, a transistor of high collector-emitter breakdown voltage is required such as the RCA 40491 which has a breakdown voltage of 300 volts. Any desired voltage can be selected across the ultimate load between 0 and 68 volts. (The basic disadvantage of a series type voltage regulator circuit is that the load

voltage is a function of the load resistance, however, the load resistance is constant in the overall circuit as will be discussed later).

The a.c. ripple smoothing ability of a capacitor is inversely related to the load current since for high load currents the resistance of the load is low and approaches the low reactance of the filter capacitors at the ripple frequency. Since C_2 is in the base circuit where the base current is about 1/50th the load (collector) current (a typical β for the type of transistor used in 50), and the base current variations control collector or load current variations, then C_2 is equivalent to a filter capacitor across the load of $C_{equiv} = \beta C_2 = 5000\mu f.$ which provides for very pure d.c. to the load by means of a $100\mu f$ filter capacitor.

The heater voltage level off circuit consists of Q_4, Q_5, C_6, C_7, R_{14}, R_{15}, D_3, D_4, D_5, D_6 and T_3. This circuit is derived from the classic full-wave silicon-controlled-rectifier motor speed-light dimmer control that can be found in any SCR Manual. This circuit appears in Figure 3.

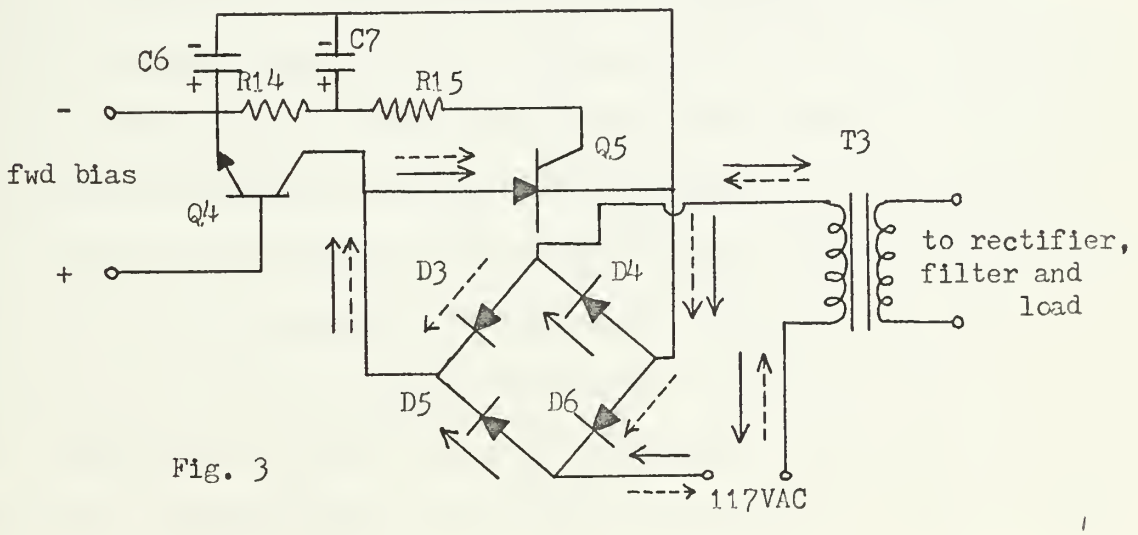

Fig. 3

D_3, D_4, D_5, and D_6 comprise a full-wave rectifier circuit so that the diode current of the SCR is in the forward direction for both halves of a 60Hz sine wave current from the 117VAC line source. Following the solid line and dotted line current direction arrows representing a.c. in Figure 3 indicate that the 60Hz line current goes through Q_5 from anode to cathode in the same direction during both halves of the sine wave current while the controlled current through the primary of T_3 is still a.c.

At this point it would be well to review the characteristics and operation of a silicon-controlled-rectifier. Silicon-controlled-rectifiers have the unique property such that the forward resistance of the diode section remains virtually infinite until a positive pulse with respect to the cathode is introduced at the SCR gate. At the instant that the pulse reaches the required trigger turn-on voltage, the forward resistance of the diode section rapidly goes to near zero (the forward current correspondingly increases commensurate with the load at a rate of 600 amperes per microsecond, i.e., SCRs turn on very rapidly) and will remain near zero until the forward current of the anode to cathode path goes below a certain holding current which is generally in the milliampere region. After the SCR has turned off due to the forward diode current decreasing to below holding current, it is necessary to again trigger the SCR gate to turn on the forward current path of the diode. With this principle of operation in mind the SCR can be triggered at the same frequency as the diode current but phase-shifted so that triggering is forced to occur at some chosen angle in the duty cycle providing a selectable RMS value of the diode current. It is the limits

of integration in determining the RMS value of current that cause the RMS value to vary by this technique.

$$I_{RMS} = \sqrt{(1/T_1)\int_{t1}^{T_1} i^2(t)\, dt} \qquad (1)$$

Figure 4 illustrates two possible choices for the integration limits.

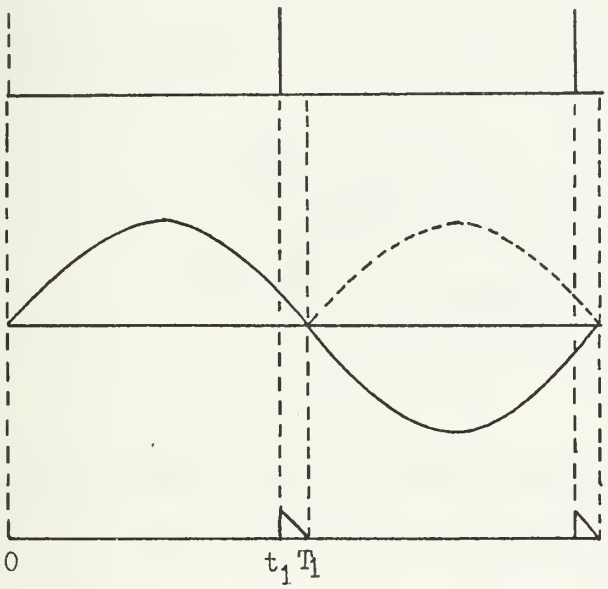

gate trigger pulses

Fig. 4a

60Hz line current (120Hz d.c.)

The negative half cycle can be made positive by using a full wave circuit.

diode current to load

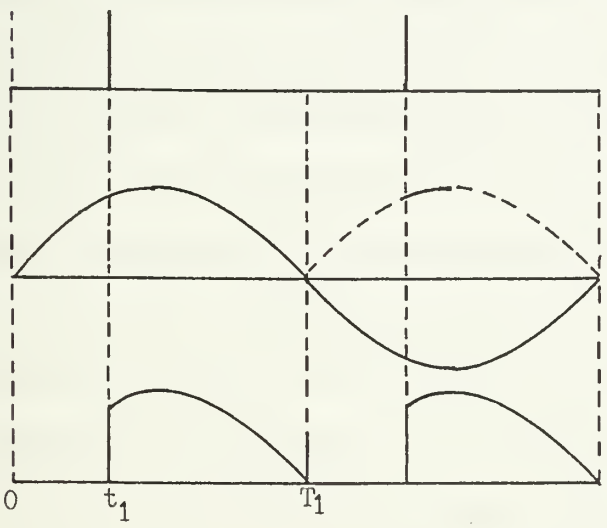

gate trigger pulses

Fig. 4b

60Hz line current (120Hz d.c.)

The negative half cycle can be made positive by using a full wave circuit

diode current to load

Fig. 4

The trigger pulses are equal in frequency to the diode load current but shifted in phase by the RC phase shift circuit comprised of C_6, R_{14}, C_7 and the collector-emitter resistance of Q_4. (R_{15} is merely a gate current limiting resistor to protect the SCR gate from excessive current drain). The collector-emitter current path of Q_4 can be thought of as a variable resistor with a value depending upon the forward bias current of the base-emitter junction of Q_4. The equivalent triggering circuit of Figure 3 is shown below in Figure 5.

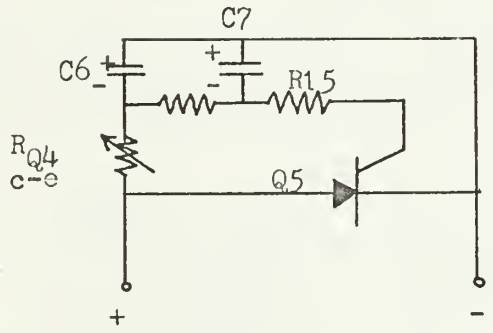

Fig.5

The phase shift that will appear across the gate-cathode circuit of Q_5 is in the range of 0 - 180° depending upon the value of R_{Q4}. When R_{Q4} is near zero, the SCR gate triggers early and will conduct for almost all of each half cycle of line current. When R_{Q4} is very large, the gate phase shift current is near 180° and the SCR triggers late in each half cycle so that the RMS current value is very small. This selectable phase change determines the lower integration limit of equation (1).

The collector-emitter resistance of Q_4, i.e., R_{Q4}, is determined by the amount of base current drawn by Q_4 which is a function of the degree of forward bias applied to its emitter-base PN junction. (See Figure 3). The level of forward bias voltage to Q_4 is determined by the conductance of the emitter-collector current path of Q_3 as illustrated by the dotted line in Figure 6.

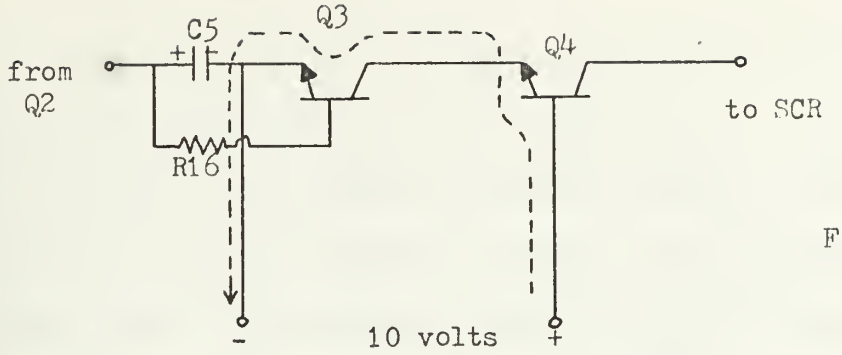

Fig.6

The emitter-collector conductance of Q_3 is in turn determined by the forward bias on its emitter-base PN junction. This forward bias voltage is the result of drainage of charge from C_5 through R_{16} as indicated by the dotted line in Figure 7.

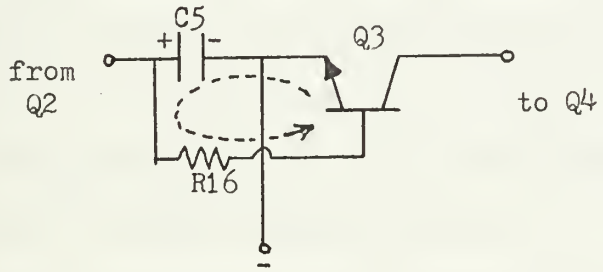

Fig.7

C_5 is charged through the emitter-collector resistance of Q_2 in series with R_{13} from the supply voltage of 10 volts (See Figure 8). (Q_6 and associated components make up a series regulated d.c. power supply of 10VDC to operate Q_2, Q_3, and Q_4). The dotted line indicates the charging current path of C_5.

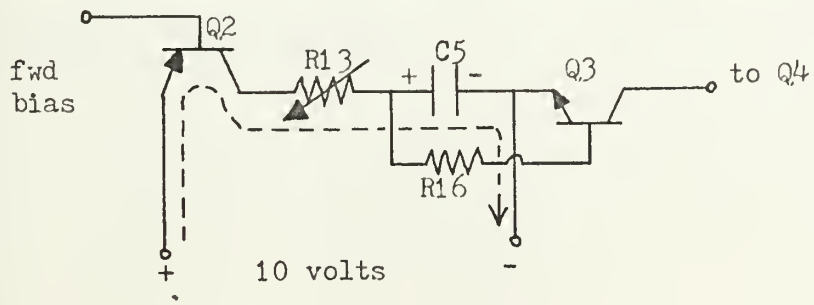

Fig.8

The series RC circuit of emitter-collector path of Q_2, R_{13}, and C_5 provide a time constant of 100 seconds maximum. This occurs when R_{13} is adjusted to its maximum resistance position. The emitter-collector resistance of Q_2 is assumed to be zero since Q_2 is operated in a saturation state. The resistance offered by R_{13} set to any value between zero and 100 kilohms is then the only resistance in the charging circuit of C_5. Since the setting of R_{13} determines the rate at which C_5 charges and consequently the point on the dynamic transfer curves that Q_3 and Q_4 are at, R_{13} determines how rapidly the secondary voltage across T_3 will rise.

Q_2 is essentially a transistor switch being either in an "off" state (cut-off base bias) or an "on" state (saturated base bias). Whether or not Q_2 is on is determined by the position of the relay contacts of RL_1 (See Figure 1). D_7, D_8, D_9, D_{10}, C_8, C_9, C_{10}, C_{11}, R_9 and R_{10} simply make up a full-wave rectifier-filter system so that the heater voltage is essentially d.c.

Since the rising heater voltage (rising at a rate corresponding to the setting of R_{13} and consequently the charge rate of C_5) and preset reference voltage are both referenced to chassis ground, there is a decreasing potential difference between the reference voltage and rising heater voltage. The "energize" coil of a suitable relay can be connected between these two points and will be energized until the potential difference decreases to below the holding voltage of the relay coil (magnet). (See Figure 9).

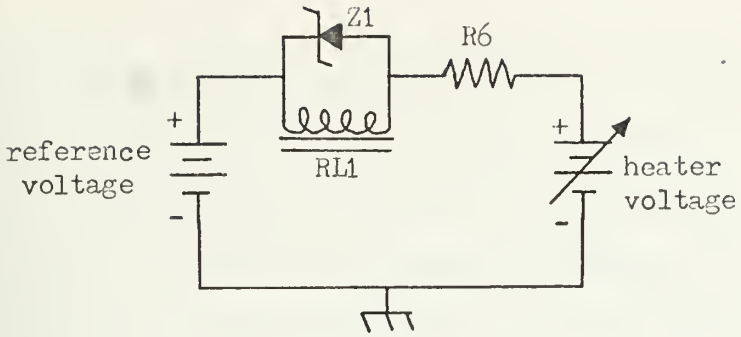

Fig.9

When this occurs the relay contacts will open up and cut off the emitter-collector current path of Q_2 since the emitter-base junction of Q_2 would no longer be forward biased (See Figure 1). R_{12} is simply a base current limiting resistor for Q_2 so that base currents are limited to about 170μa. which is more than adequate to drive Q_2 into saturation.

When the difference between heater voltage and the reference voltage goes to 3.5 volts, the holding voltage of RL_1, the relay will de-energize, Q_2 will be cut off, C_5 will stop charging, Q_3 and Q_4 will maintain their respective emitter-collector resistance in agreement with the potential left across C_5 and the SCR will trigger at the same place in the SCR diode circuit load current. Hence, the voltage across the secondary (and the primary) of T_3 will stop rising. This leveling off of heater voltage will maintain itself until the charge drainage of C_5 through R_{16} and the emitter-base junction of Q_3 causes the base current of Q_3 to begin to decrease. However, since the time constant of R_{16} and C_5 in series with the Q_3 emitter-base junction resistance is slightly greater than 1000 seconds, the level-off heater voltage will maintain itself for several minutes before a decrease in heater voltage becomes apparent. R_{16} contributes only to the drainage of C_5 and not to its charging and R_{13} contributes only to the charging of C_5 and not its

drainage so that C_5 can be charged as rapidly or as slowly as desired and not affect the drainage time constant.

The series resistor, R_6, only limits the relay magnet current to a safe level when the potential difference between heater voltage and reference voltage is a maximum. This maximum could be as high as 68 volts (when heater voltage is zero and depending upon the setting of R_2). The relay used clicks down at 10.5 volts and lifts up at 3.5 volts. It can safely withstand a continuous duty voltage of 26 volts. Z_1 in series with R_6 limits the voltage across the relay coil to 13 volts at all potential differences between reference supply and heater supply until of course, the actual difference decreases to a value below 13 volts. The relay coil is protected at all times by the zener properties of Z_1.

The power delivered to the film-heater can be obtained by monitoring the voltage across the film on an oscilloscope. Assuming the resistance of the film to be constant, $P = V^2/R$. The resistance of the film used was 200 ohms so that $P = V^2/200$.

R_4, Z_2, C_4, and R_8 along with the 68 volts available from the reference voltage power supply comprise the necessary circuitry for constantly monitoring the germanium resistance. (See Figure 1).

Z_2 is a 4 volt zener diode which causes a constant voltage of 4 volts to be dropped across itself. R_4 is a current limiting resistor for Z_2 so that 64 volts can be dropped across R_4 while 4 volts is maintained across Z_2. If for some reason the supply voltage should drop to 50 volts, then 4 volts will still be dropped across Z_2 and 46 volts will be dropped across R_4 automatically. C_4 provides for added

ripple filtering so that pure d.c. is used to make the germanium resistance measurements. The combination of R_4, Z_2, and C_4 can be thought of as a 4 volt battery. R_8 is a very low tolerance resistor in series with the germanium so that the germanium and R_8 form a voltage divider network. An oscilloscope (vertical deflection) is connected across R_8 so that the actual voltage across the germanium can be measured.

It was determined early in the design of this apparatus that germanium no longer behaves in an ohmic manner at 4.2°K. For this reason, both germanium current and voltage must be measured, or at least included into the resistance calculation of the germanium. The equivalent circuit of the germanium resistance measuring circuit is illustrated in Figure 10.

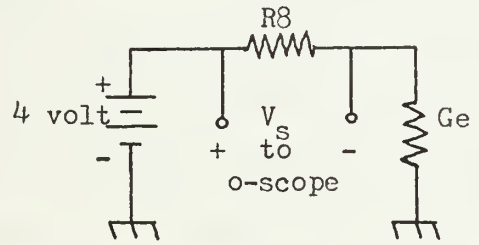

Fig.10

The germanium resistance can be found directly from the measurement of the voltage across R_8.

$$R_{Ge} = V_{Ge}/I_{Ge} = (4 - V_s)/(V_s/20K\Omega)$$

$$R_{Ge} = 20\left(\frac{4}{V_s} - 1\right) \text{ kilohms}$$

A 200μa. full scale panel meter is used to measure reference voltage and heater voltage (not simultaneously). The internal resistance of the meter is 550 ohms. The meter, in the capacity used here is that of a voltmeter with a full scale reading of 200 volts. In order to make 200 volts bring the meter to a full scale reading of 200, the meter must draw 200μa. This requires a series resistance of one megohm.

As illustrated in Figure 1, all switches are shown such that germanium resistance can be measured and reference voltage can be selected. All other circuits are turned 'off'. S_3 in the position shown ensures that the voltage across C_5 starts from zero at t = 0. As S_3 is thrown to the opposite position, T_2 and the heater voltage rise-rate circuits are energized. C_5 can now charge since it is no longer shorted and so can the heater voltage filter capacitors, C_8, C_9, C_{10}, and C_{11}. When S_3 is then returned to its original "off-heat" position, the heater voltage is returned to zero immediately. This would not be the case if the heater voltage filter capacitors were not directly shorted out. Likewise, the voltage across C_5 is immediately reduced to zero so that the charging of C_5 for the next heating cycle will always start with the voltage across C_5 equal to zero.

3.3 Instrumentation Operation

It should be apparent from the above discussion that the operation of this device is quite simple due to the built-in automation of the system. Heat speed is controlled by the value of R_{13} located at the rear apron of the equipment chassis. (See Figure 12). Reference voltage or

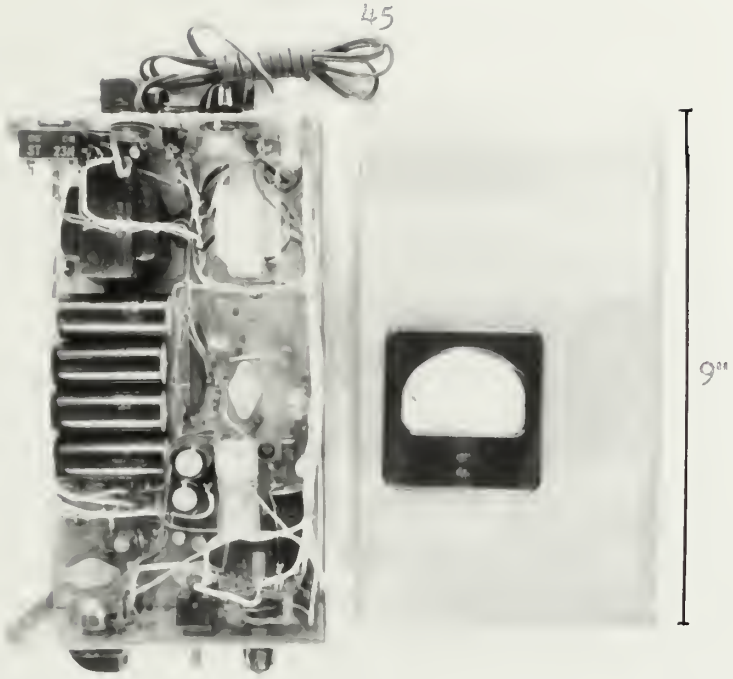

Fig. 11

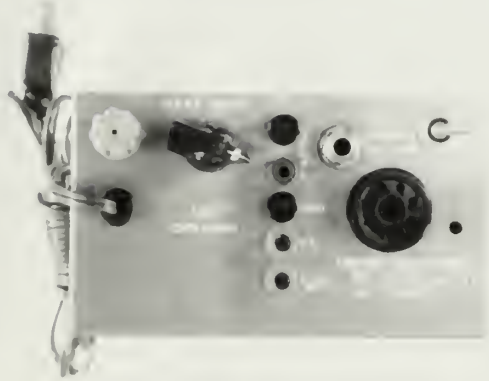

Fig. 12

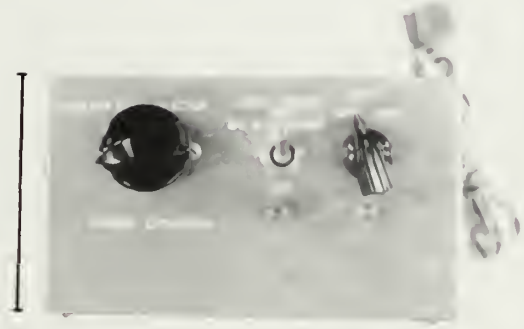

Fig. 13

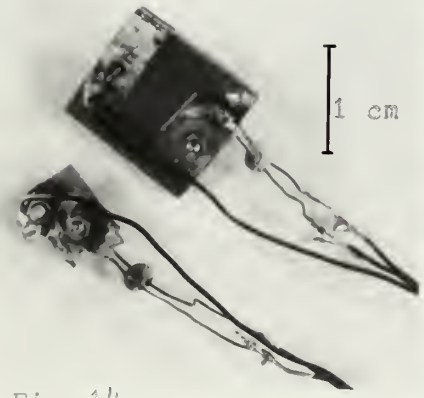

Fig. 14

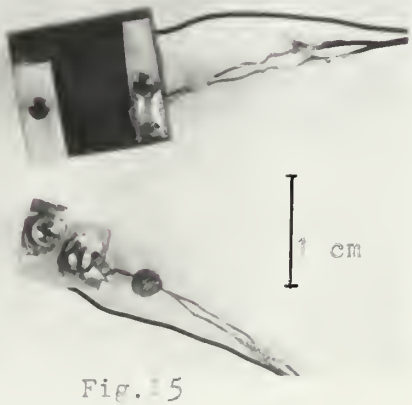

Fig. 15

heater level-off voltage is set by putting the meter switch, S_2, in the appropriate position and adjusting R_2 to the required value. R_2 is located as shown in Figure 13.

Electrical connections from the stannous-oxide-germanium wafer are made as shown in Figures 1 and 12. Germanium resistance measurements alone are made by turning on the main power switch, only (S_1). (See Figure 13). Heat is applied at the chosen rate by turning S_3 to the opposite position shown in Figure 1 (See also Figure 13). Cooling of the sample is obviously achieved by returning S_3 to its former position.

Note that T_3 is external to the rest of the chassis and all other components. This is because the value of stannous-oxide resistance will dictate what upper limit of heater voltage is required to reach the desired annealing temperature. The transformer for T_3 used with the larger wafer as shown in Figures 14 and 15 has a secondary voltage of 48 volts RMS. The film resistance is nominally 200 ohms. Should a film resistance of say 100 ohms be used on a different wafer, then T_3 must have a secondary voltage of at least 27.6 volts RMS since 15 watts are necessary to heat a sample of this size to 270°K (assuming that this is the desired annealing temperature), i.e., $V^2_{RMS} = PR/2$. About 277 ohms is the upper limit of film resistance to which the apparatus can supply at least 15 watts since the upper limit of heater voltage available is equal to the reference supply voltage less the relay lift-up potential or 64.5 volts. The automation circuits will limit the voltage to the primary of T_3 to that required to bring the heater voltage to 64.5 volts and no more. In light of this, it would be impossible to try to force higher voltages by using a much higher voltage secondary winding capability for T_3 than 45.6 volts RMS, i.e., $64.5/\sqrt{2}$.

CHAPTER IV

RESULTS AND CONCLUSIONS

4.1 Results

Extensive out-of-pile tests have been performed in heating the larger of the two assemblies shown in Figures 14 and 15 in Chapter III to various elevated temperatures as high as 270°K. while the assembly was immersed in liquid helium.

Figures 1 through 23 illustrate various heating rates and annealing temperatures of the germanium by the stannous-oxide film corresponding to selected rates of heater voltage rise and heater hold voltage. The cooling rates in general should be about the same regardless of heating rate and annealing temperature since cooling is achieved simply by removal of the heater voltage. It is apparent however, that there are differences in cooling rates, since the rate of cooling experimentally turned out to be a function of annealing temperature or the temperature at which cooling had begun.

In Figures 1 through 30, the upper curve is the curve of germanium resistance and the lower curve is that of heater power. The abscissa is time. The ordinate scales are not linear in their units since neither heater power nor germanium resistance is linearly related to the heater or germanium voltage, respectively.

$$P = V^2/200 \text{ watts}$$

$$R_{Ge} = 20\left(\frac{4}{V_s} - 1\right) \text{ kilohms}$$

Figures 1 through 30 were taken by photograph on a Tektronix Model 564 Dual Trace Storage Oscilloscope.

Figure 31 is a rough conversion curve of germanium resistance to temperature based on three known points: 270°K, 80°K (liquid nitrogen) and 4.2°K (liquid helium).

Table 1 is a summary of the results shown in Figures 1 through 30 indicating germanium temperatures, heater powers and times of interest to be discussed further in the following.

Figures 1 and 3 show that rapid heating and cooling of the sample, the primary objectives of the experiment, were sucessfully achieved. From Figure 1 it is seen that the germanium resistance falls from 380 kilohms (4.2°K) to about 40 kilohms (150°K) in 35 milliseconds, and reaches 12 kilohms (270°K) in about one second. By comparison Figure 4, illustrating a heating rate to 270°K chosen to be not as great as that of Figures 1 and 3, shows that 40 kilohms (150°K) is reached in 100 milliseconds. 12 kilohms (270°K) is reached in about two seconds. Further comparison shows that Figure 5, the third fastest heating rate to 270°K chosen, takes about three seconds to reach 270°K. The fourth fastest heating rate (Figure 6) reaches 270°K in about 3.5 to 4 seconds. The slowest heating rate that the instrumentation can provide (Figure 7) allows the sample to reach 270°K in about 4 seconds. (Controlled heating rates may be desirable in some annealing experiments). The heater power curves are not modulation free since pure direct current is not achievable without sacrificing response time, i.e., increasing the time constant of the heater power filtering circuit comprised of C_8, C_9, C_{10}, and C_{11} of Figure 1, Chapter III. It is deemed that response time is far

TABLE 1

Heating rate	fastest			second fastest			third fastest			fourth fastest			slowest		
Final temp. (Degrees K)	270	190	165	270	190	165	270	190	165	270	190	165	270	190	165
Heating Rise time to 40KΩ (150°K) (milliseconds)	35	50	*	100	150	50	100	200	*	150	150	*	200	160	*
Heating Rise time to final temp. (milliseconds)	1000	300	*	2000	600	200	3000	2000	*	3700	2500	*	4000	800	*
Cooling Fall time to 380KΩ (4.2°K) (milliseconds)	1180	340	*	1150	250	8	1000	280	*	900	250	*	700	*	*

* no data

more important than obtaining pure direct current for the heater since the germanium resistance curves do not experience a similar modulation.

Upon cooling from 270°K to 4.2°K, there is a distinct delay after the heater power is turned off. There is a variation in cooling time between 1.2 second and 0.7 second depending upon how rapidly the specimen was heated to 270°K. In Figure 2, achieving 270°K at the fastest rate, cooling time was 1.18 second while Figure 5, the third fastest heating rate chosen, shows a cooling time of one second. The slowest heating cycle cooling time as evidenced by Figure 7 shows that about 0.7 second was needed. A possible explanation of the relationship between two otherwise unrelated events, i.e., heating and cooling, is that of the degree of turbulence set up in the liquid helium surrounding the vapor bubble during the transition from nucleate to film boiling. A greater heating rate yields a time derivative of the temperature gradient of the helium surrounding the sample that is not zero. i.e., heat transfer to the helium is not given sufficient time to reach steady-state, hence a greater turbulence results which will cause an increase in convected heat from the germanium. Since the liquid helium system was not allowed to come to steady-state before cooling had been begun, the convective flow of heat had not been minimized. It is expected that if the sample were held for a greater length of time at the chosen annealing temperature before cooling so that convective heat flow can be minimized, the cooling rates would be more nearly the same regardless of heating rate.

Figures 8 through 23 are curves similar to Figures 1 through 7 but are for annealing temperatures less than 270°K. Figures 8 and 10 are

illustrations of the fastest heating rate to a germanium resistance of about 28 kilohms (190°K) from 380 kilohms (4.2°K). Heating to 40 kilohms (150°K) takes about 50 milliseconds. Continued heating to 28 kilohms (190°K) requires approximately an additional 250 milliseconds. Figures 11 and 13, showing the rate of germanium resistance decrease by means of the second fastest heating power rise, illustrate that about 150 milliseconds are required to reach 40 kilohms (150°K). 28 kilohms (190°K) is reached in about 0.6 second. The third fastest heating rate to 190°K chosen, shown in Figures 14 and 16, indicate a rise time to 40 kilohms (150°K) of 200 milliseconds. 28 kilohms (190°K) is eventually achieved in about two seconds. Figures 17 and 19 showing the fourth most rapid heating to 28 kilohms (190°K), indicate that 150 milliseconds are required to reach 40 kilohms (150°K). 28 kilohms (190°K) is reached in a total of 2.5 seconds. The slowest heating rate to 28 kilohms (190°K) is shown in Figure 20. 160 milliseconds are needed to heat to 40 kilohms (150°K). To reach 28 kilohms (190°K) a total heating time of 0.8 second is required. The instability of germanium resistance as shown in this figure illustrates the formation and collapse of the helium vapor bubble surrounding the quartz-germanium assembly. Heating through the critical temperature for the transition of nucleate boiling to stable film boiling results in the bubble instability and hence the instability in germanium temperature and resistance.

Looking at the cooling phase of various heating rates to 28 kilohms (190°K), Figure 9 shows that 340 milliseconds are required to cool the specimen back to 380 kilohms (4.2°K). By comparision Figure 2, illustrating the cooling rate from 270°K to 4.2°K required 1.18 seconds!

250 milliseconds are needed to cool the specimen back to 4.2°K from 190°K for the case when the second fastest heating to 190°K was employed. (See Figure 12). Figure 15 shows that 280 milliseconds are needed for the cooling after heating slower than the heating rate used in Figure 12. One would expect the cooling times in the latter two cases to be reversed but for the reasons of liquid helium turbulence stated previously, i.e., length of time held at 190°K, they are not. Figure 18 indicates that 250 milliseconds are needed to cool the specimen from 28 kilohms (190°K) to 380 kilohms (4.2°K).

Heating-cooling cycles were also performed for an annealing temperature of about 165°K (35 kilohms) using the fastest to the slowest heating rates. At a hold temperature as low as this, the ratio of duty current for each cycle to the whole cycle of current through the SCR is much less than this ratio for higher annealing temperatures (heater voltages). For this reason the "on time" of the SCR is short enough to allow observable decay of the heater voltage filter circuit as evidenced by the sawtooth pattern of the heater power illustrated in Figures 20 through 30. Since the frequency response of the instrumentation is lower than the heat flux from the sample to the liquid helium, the bubble formation and collapse is more evident in these figures as unstable-film-boiling occurs. This phenomena is illustrated by the tendency for the germanium resistance curves in Figures 20 through 30 to ride the heater power peaks and valleys. A successful attempt was made to find the critical heater power per unit surface area of heat conduction of the germanium-quartz wafer in order to cause the transition from nucleate boiling to film boiling. According to Bowman[10] the maximum surface

temperature rise in nucleate boiling is less than one degree. This minute change cannot be distinguished on Figures 1 through 29. Figures 24 through 28 show that about three watts of heater power are necessary to cause a discernible temperature rise (resistance decrease) of the germanium. This temperature increase indicates the transition from nucleate to film boiling. The required specific heater power to cause the transition is therefore the ratio of critical heater power to the heat conduction cross-sectional area of the wafer (two sides). This is shown to be:

$$\frac{3 \text{ watts}}{2 \times 1.44 \text{ cm}^2} = 1.04 \text{ watt/cm}^2$$

This is in agreement with Bowman's experiment.

The instability of heater power shown in Figures 16, 17, and 19 is a result of unstable SCR triggering. The reason for this jog in the exponential rise in heater voltage is not known. However, after the instability is passed, the heater voltage continues to rise as before to its predetermined value. Experiments have shown that this instability exists only at this particular chosen power increase rate. Those rates chosen to be faster or slower do not exhibit this instability. It is well to note that the instability occurs at a high enough heater voltage output such that the boiling regime does not become unstable. For this reason, the heater voltage instability is of little concern since it is at least consistent.

Figure 30 indicates that a specific heater power of less than 1 watt

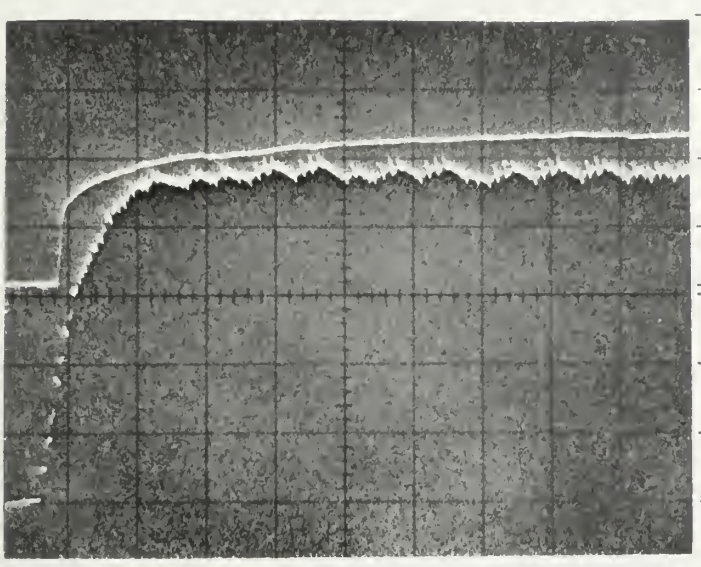

Fig. 1
Fastest heating to 270°K
(heating)
Hor. scale 0.2sec/cm

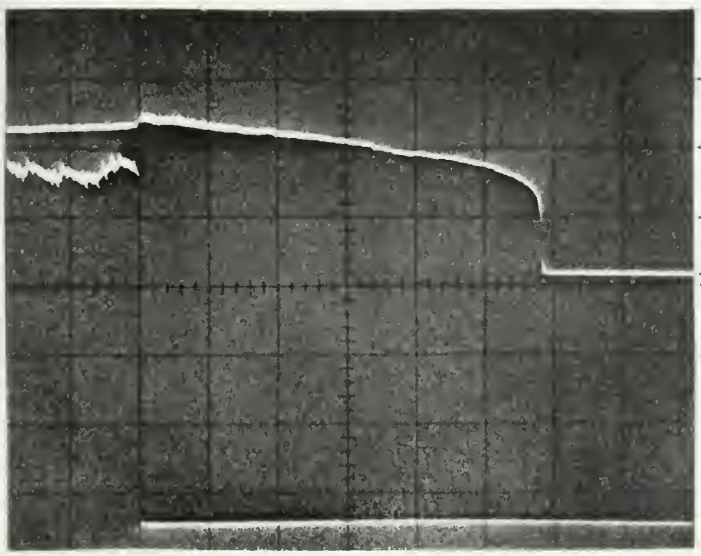

Fig. 2
Fastest heating to 270°K
(cooling)
Hor. scale 0.2sec/cm

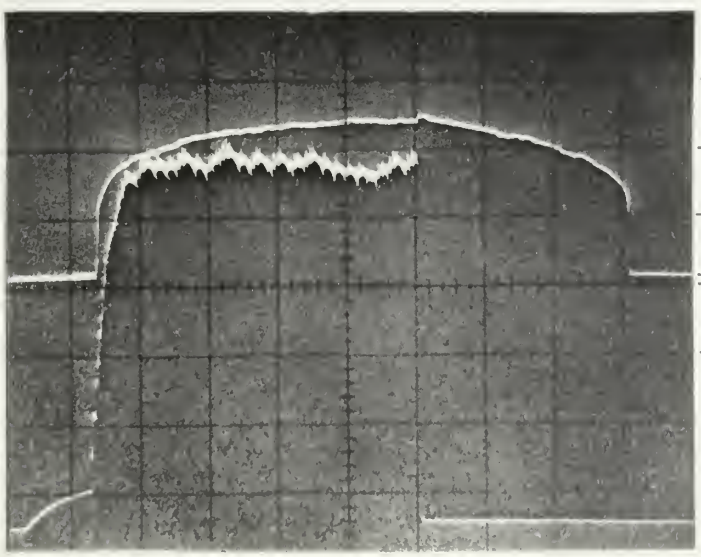

Fig. 3
Fastest heating to 270°K
(whole cycle)
Hor. scale 0.5sec/cm

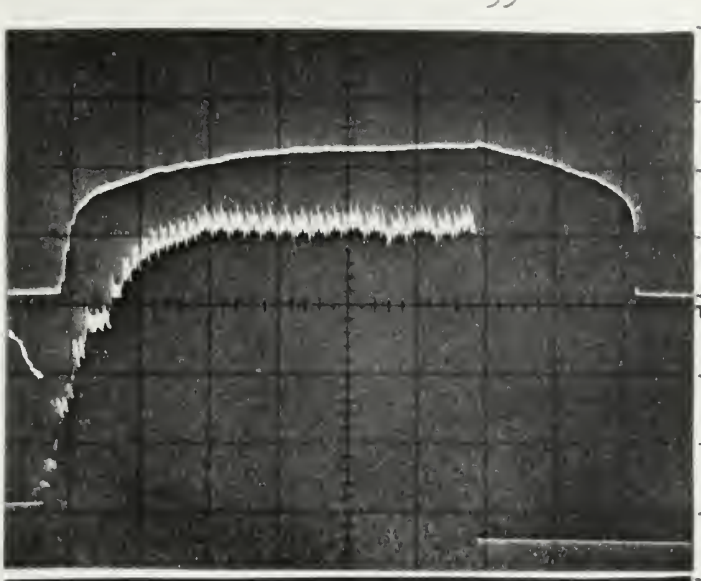

Fig.4
Second fastest heating to 270°K

(whole cycle)

Hor. scale 0.5 sec/cm

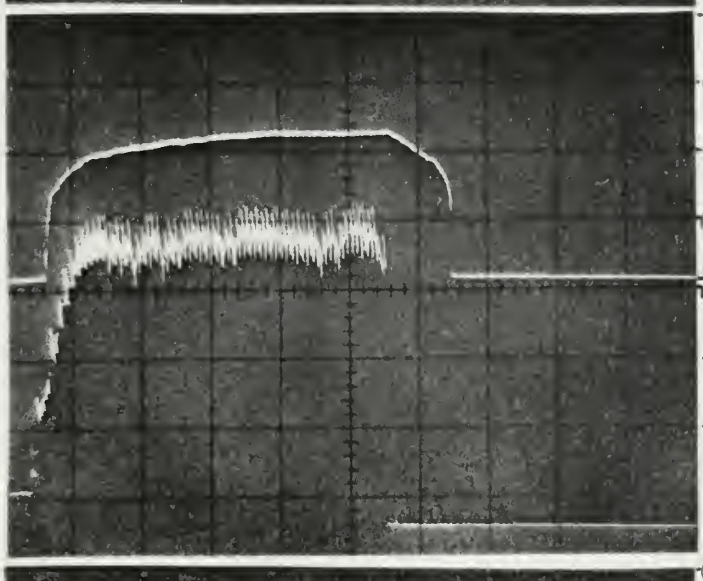

Fig.5
Third fastest heating to 270°K

(whole cycle)

Hor. scale 1 sec/cm

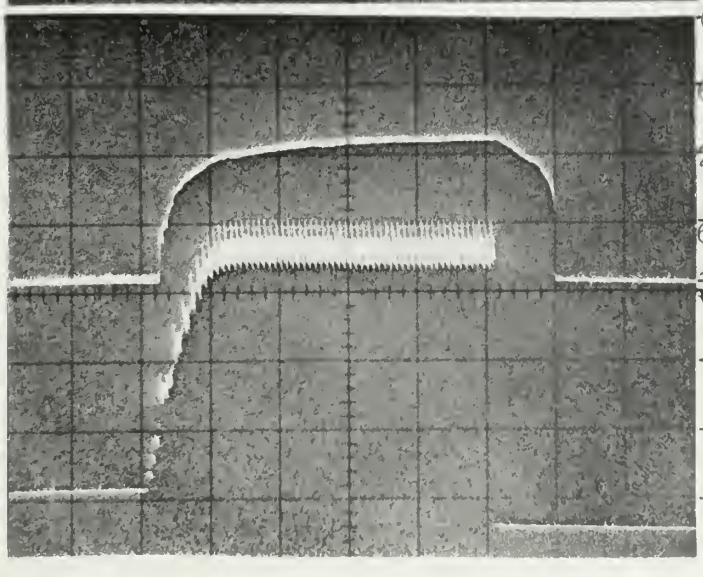

Fig.6
Fourth fastest heating to 270°K

(whole cycle)

Hor. scale 1 sec/cm

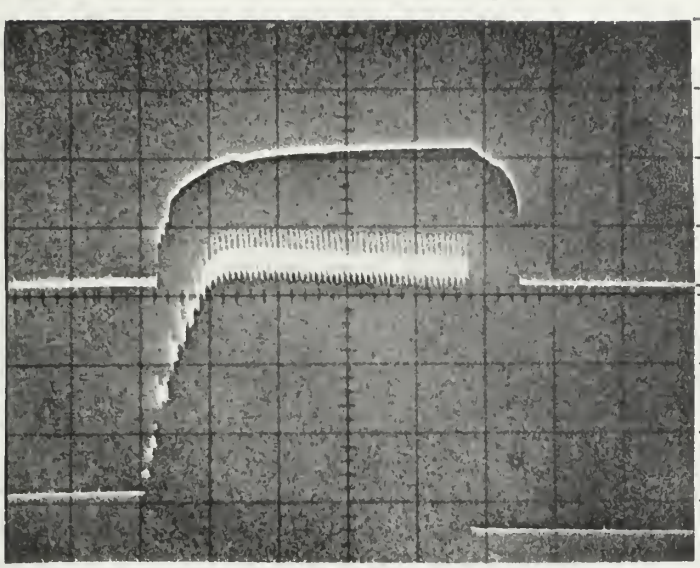

Fig.7
Slowest heating to 270°K

(whole cycle)

Hor.scale 1 sec/cm

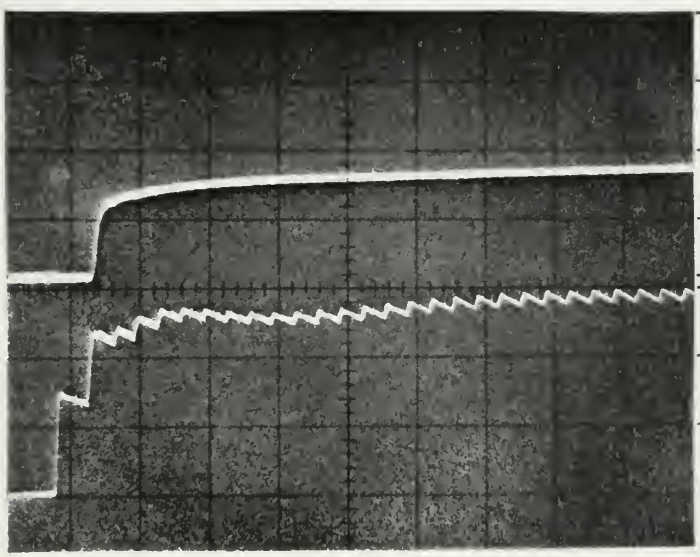

Fig.8
Fastest heating to less than 270°K

(heating)

Hor.scale 50msec/cm

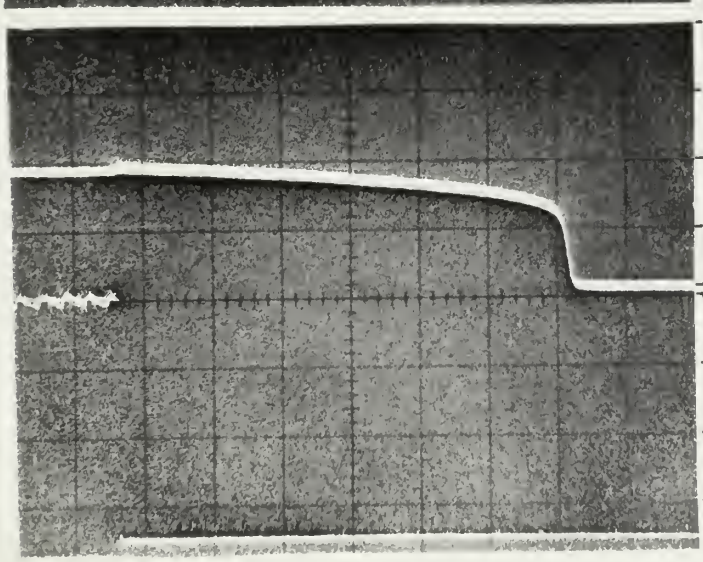

Fig.9
Fastest heating to less than 270°K

(cooling)

Hor.scale 50msec/cm

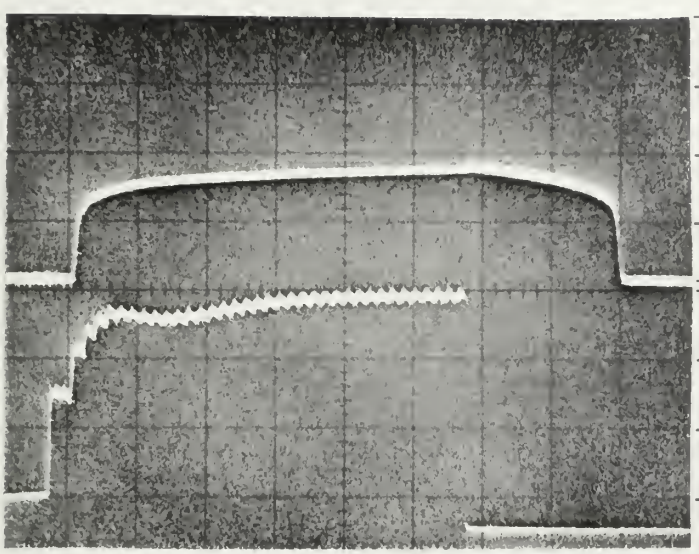

Fig.10
Fastest heating to less than 270°K
(whole cycle)
Hor.scale 0.1sec/cm

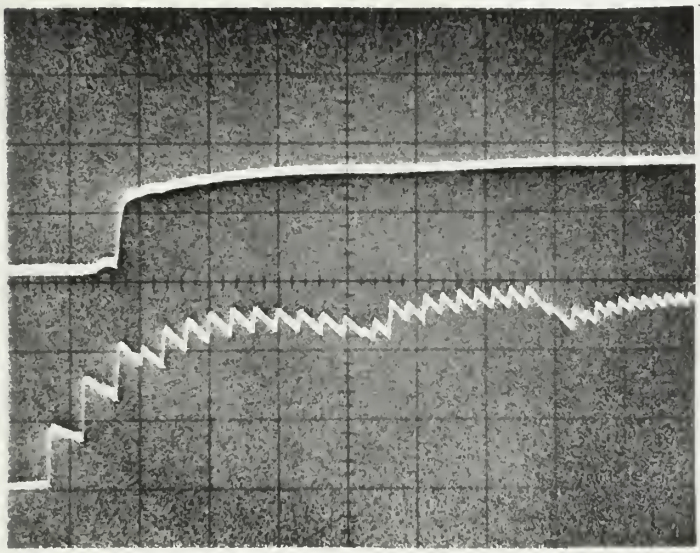

Fig.11
Second fastest heating to less than 270°K
(heating)
Hor.scale 0.1sec/cm

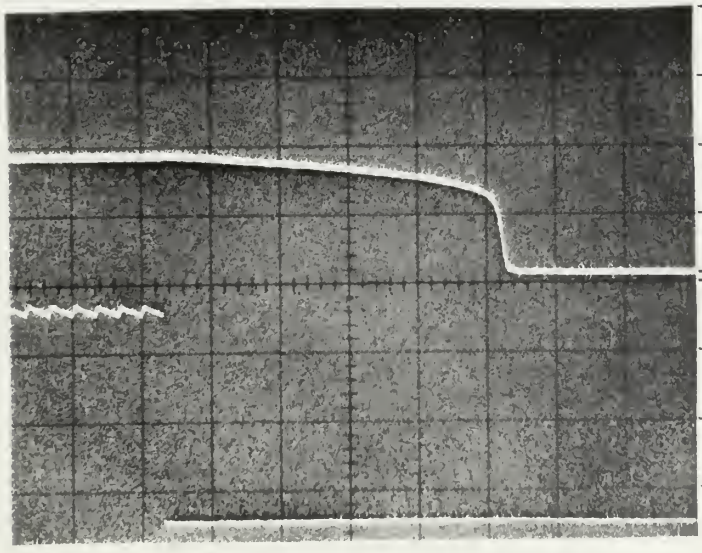

Fig.12
Second fastest heating to less than 270°K
(cooling)
Hor.scale 50msec/cm

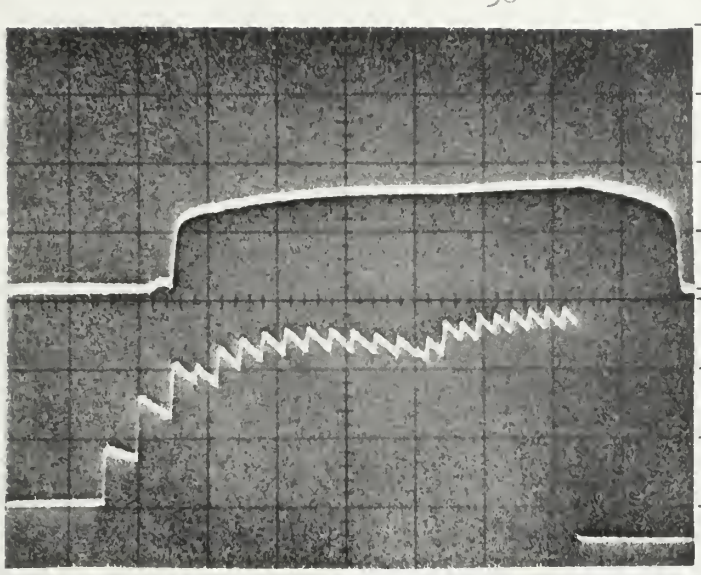

Fig.13
Second fastest heating to less than 270°K

(whole cycle)

Hor.scale 0.1sec/cm

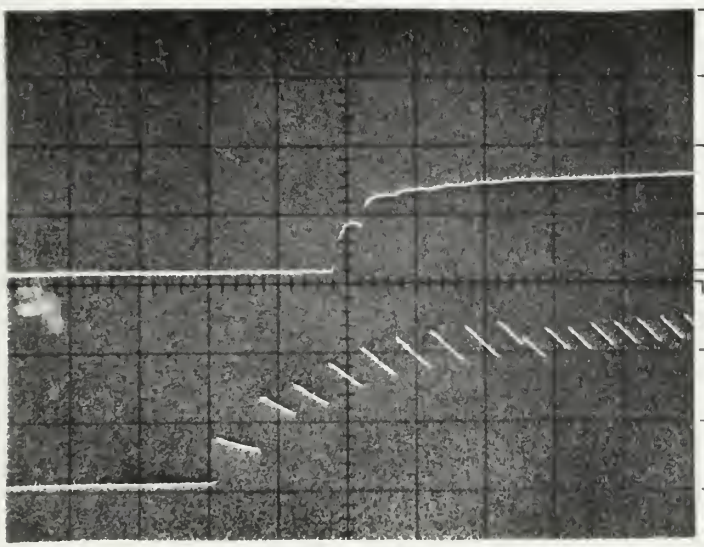

Fig.14
Third fastest heating to less than 270°K

(heating)

Hor.scale 0.1sec/cm

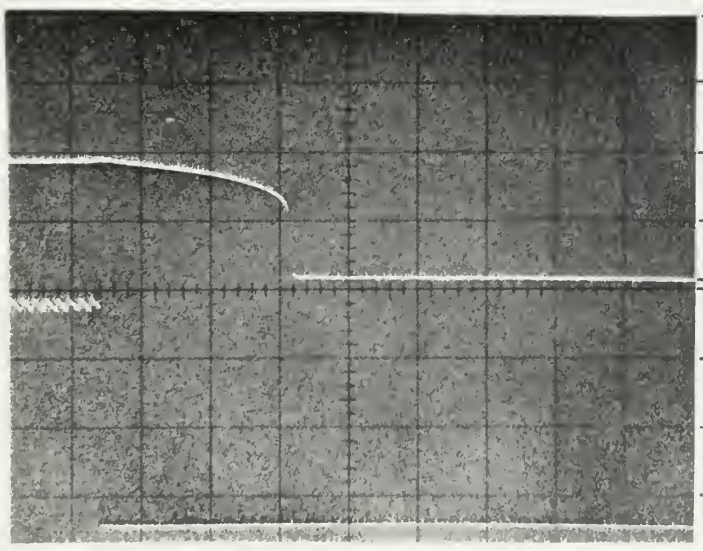

Fig.15
Third fastest heating to less than 270°K

(cooling)

Hor.scale 0.1sec/cm

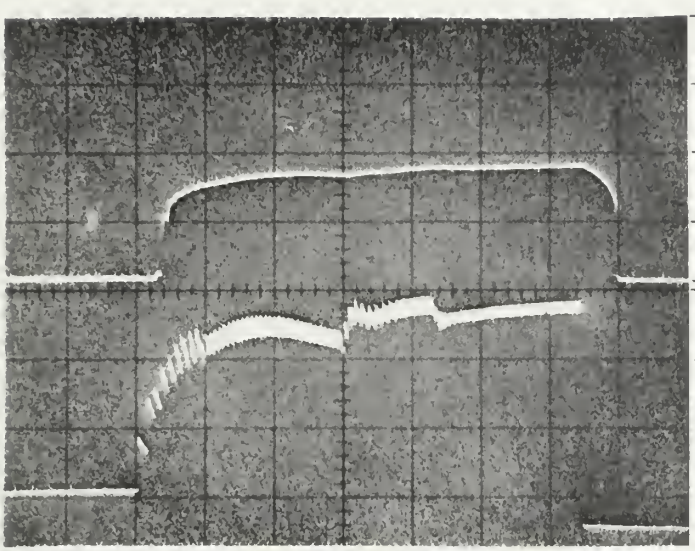

Fig.16
Third fastest heating to less than 270°k

(whole cycle)

Hor. scale 0.5sec/cm

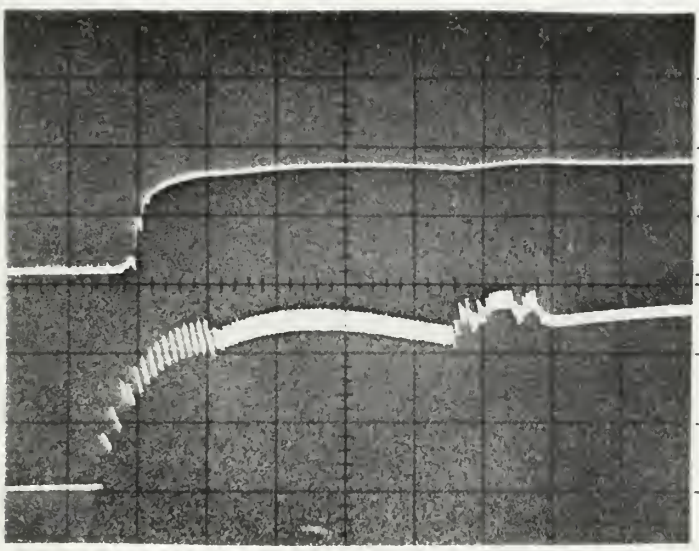

Fig.17
Fourth fastest heating to less than 270°K

(heating)

Hor. scale 0.5sec/cm

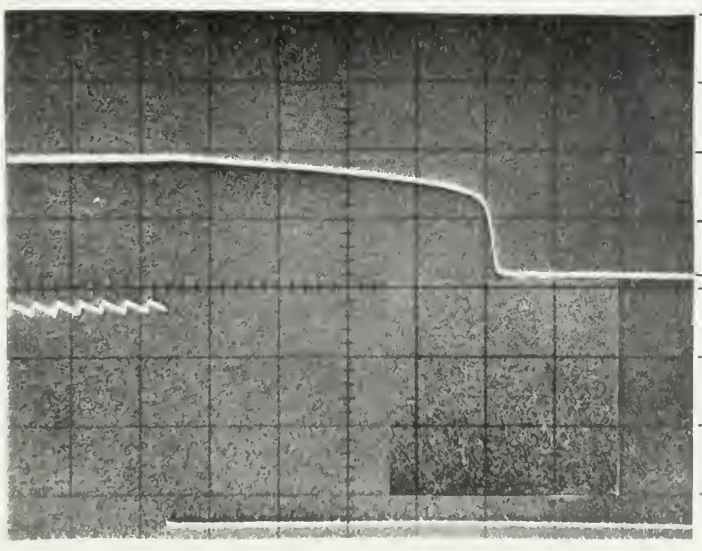

Fig.18
Fourth fastest heating to less than 270°K

(cooling)

Hor. scale 50msec/cm

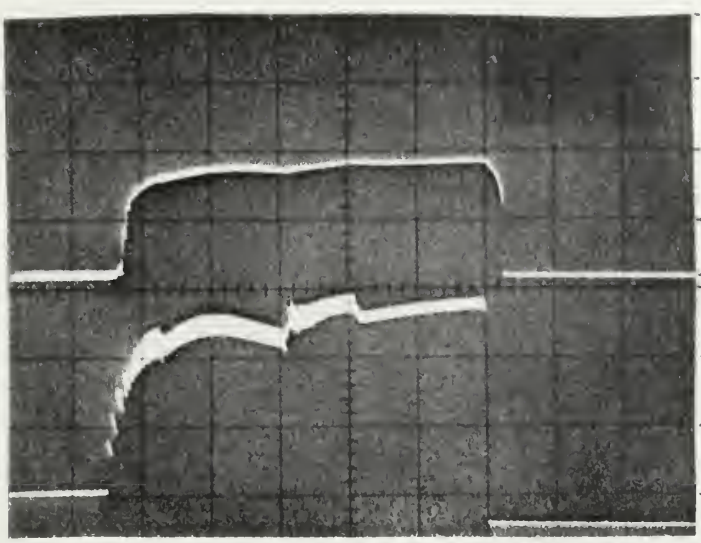

Fig.19
Fourth fastest heating to less than 270°K

(whole cycle)

Hor.scale 1sec/cm

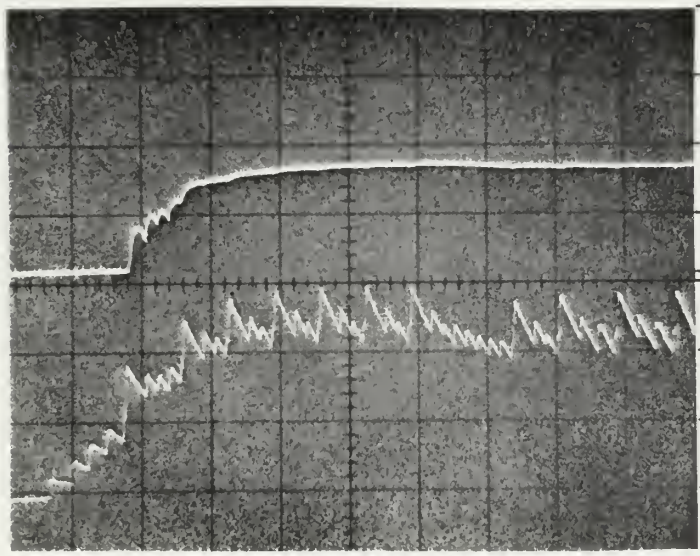

Fig.20
Slowest heating to less than 270°K

(heating)

Hor.scale 0.2sec/cm

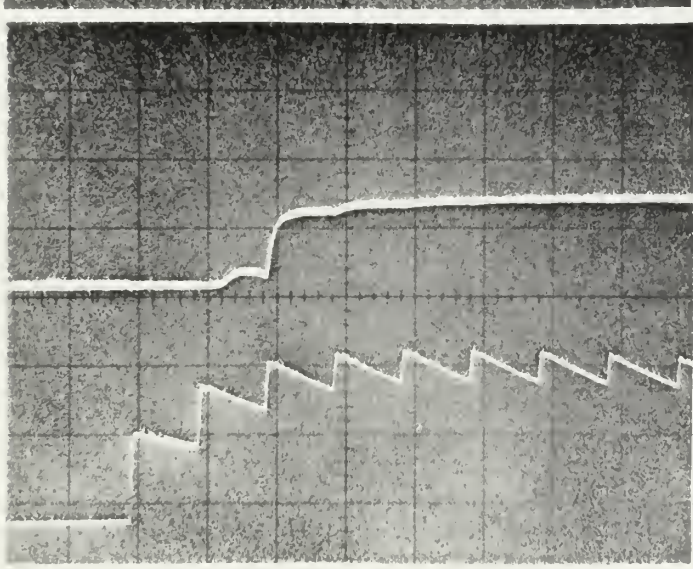

Fig.21
Second fastest heating to much less than 270°K

(heating)

Hor.scale 50msec/cm

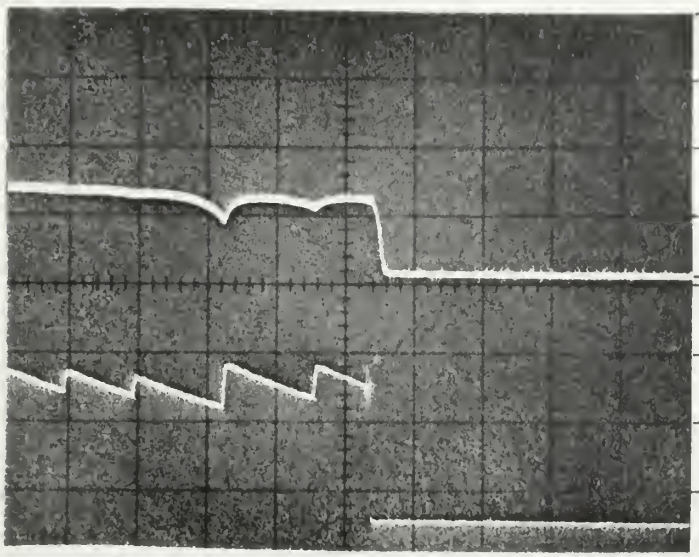

Fig.22
Second fastest heating to much less than 270°K (cooling)
Hor. scale 50msec/cm

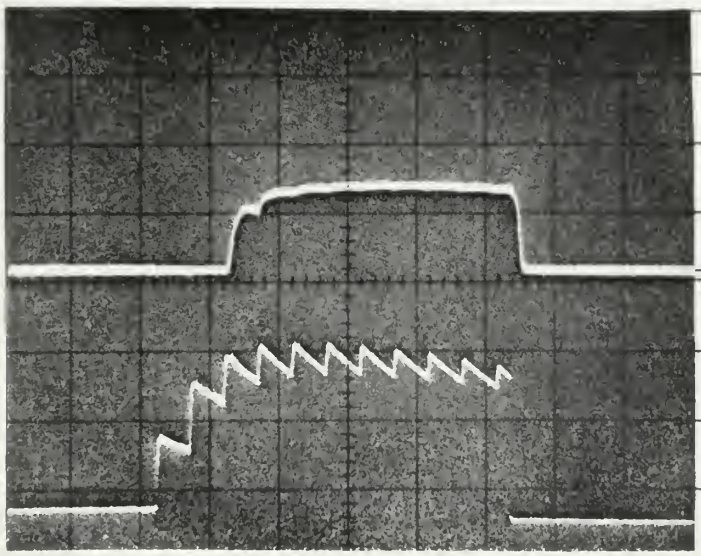

Fig.23
Second fastest heating to much less than 270°K (whole cycle)
Hor. scale 0.1sec/cm

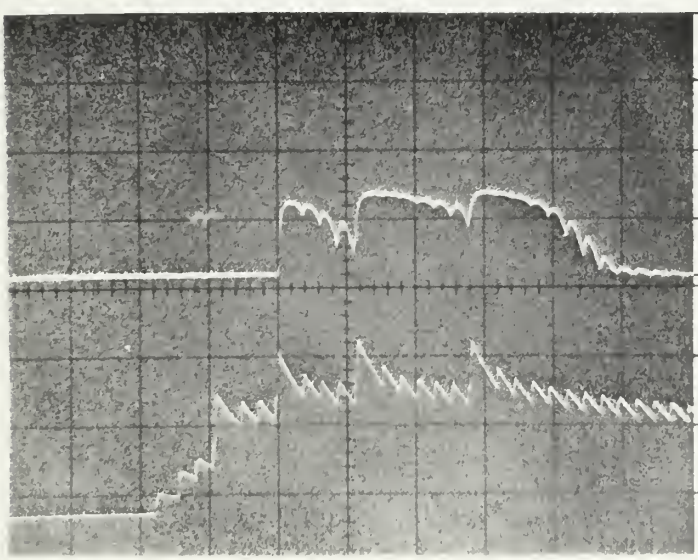

Fig.24
Slowest heating to about vapor bubble threshold temp. (heating)
Hor. scale 0.2sec/cm

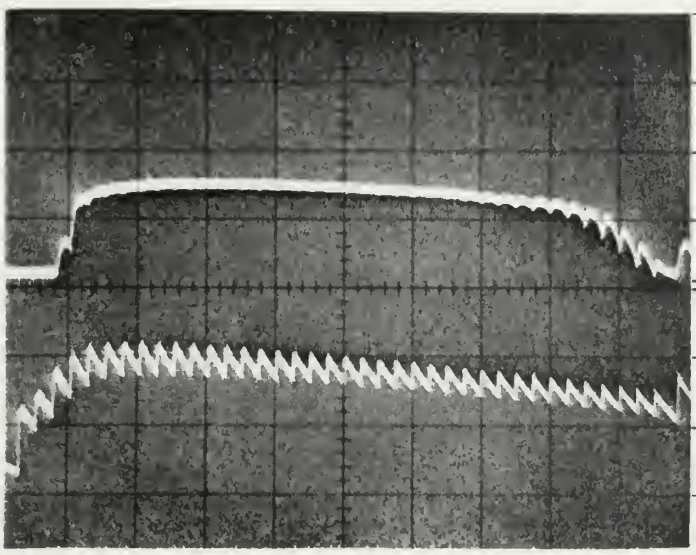

Fig.25
Slowest heating. Illustrates bubble collapse.

Hor.scale 0.2sec/cm

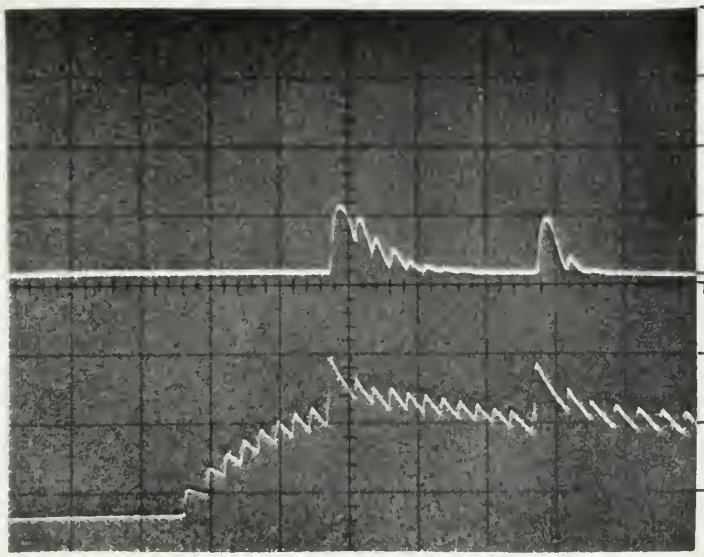

Fig.26
Slowest heating at vapor bubble threshold temp.

(heating)

Hor.scale 0.2sec/cm

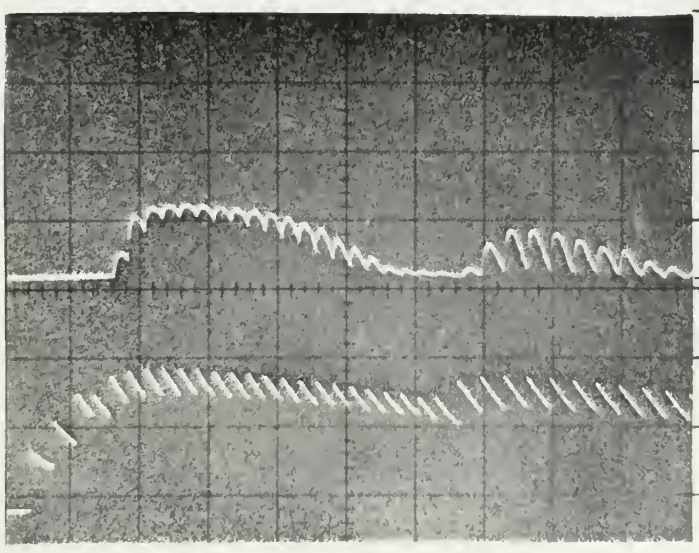

Fig.27
Fourth fastest heating to vapor bubble threshold temp.

(heating)

Hor.scale 0.2sec/cm

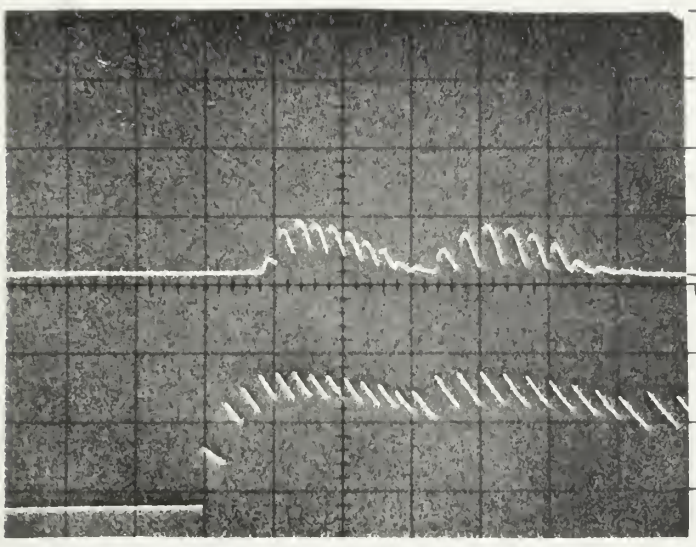

Fig.28
Third fastest heating. Illustrates vapor bubble collapse.

(heating)

Hor. scale 0.2sec/cm

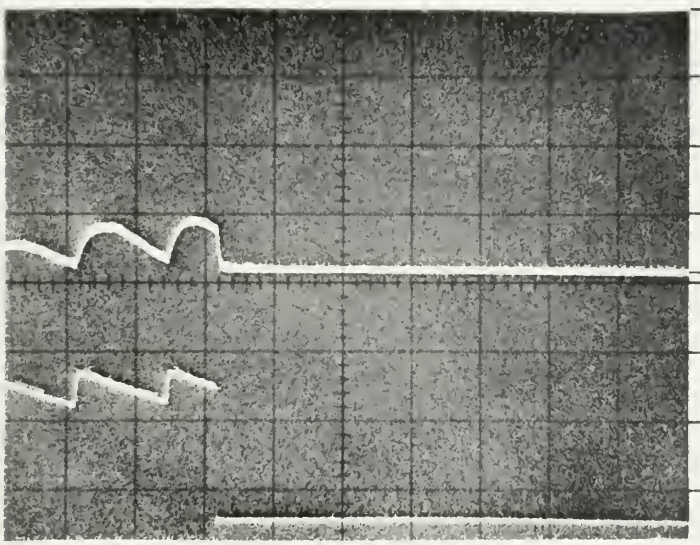

Fig.29
Same as Fig.28, except Hor. scale

50msec/cm

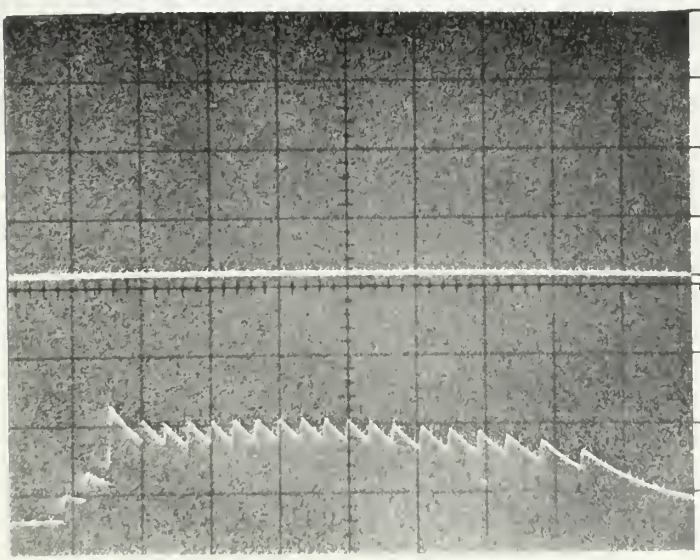

Fig.30
Slowest heating to below vapor bubble threshold temp.

Hor. scale 0.2sec/cm

Germanium Temperature Vs. Resistance

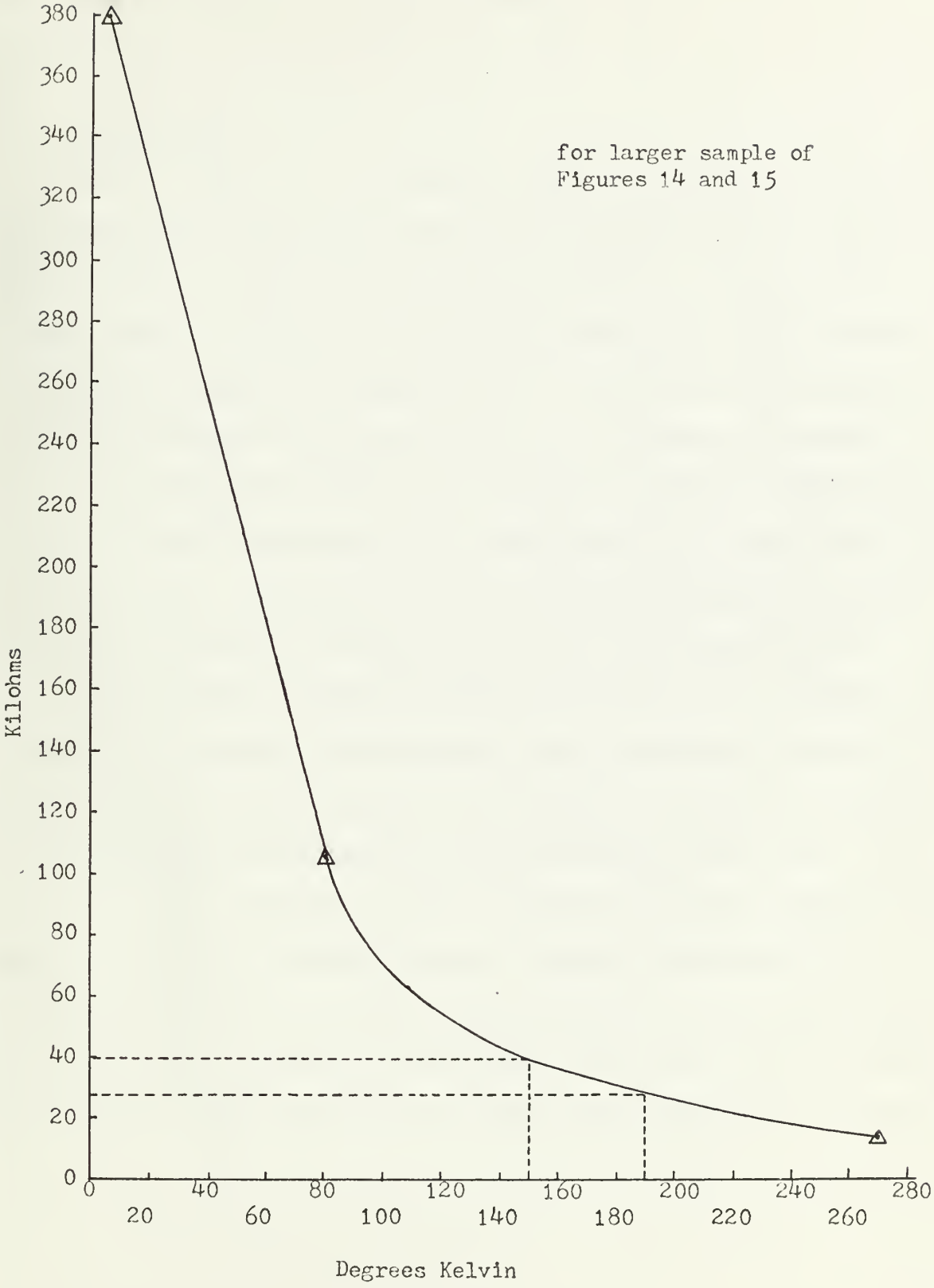

Figure 31

per cm^2 positively is not enough to change from nucleate boiling to film boiling.

4.2 Conclusions

Since the mass of the two samples shown in Figures 14 and 15 are very small, the in-pile gamma heating will contribute to less than one watt in fifteen toward heating the sample to 270°K. The mass of the larger sample is 1.38 gram and the gamma heating is one watt per gram, therefore the sample will require 1.38 watt less to cause heating to an elevated temperature when in-pile than what is indicated by Figures 1 through 23. Since the critical power required to heat the larger sample to film boiling is three watts, the gamma heating alone cannot cause film boiling to occur. Therefore, the germanium temperature can be lowered to within a fraction of a degree to the liquid helium temperature.

The out-of-pile experiment undertaken has proven that a working specimen and associated instrumentation can be constructed to meet the rapid heating and cooling requirements necessary to carry out the actual in-pile simulation of higher than the environmental neutron flux. As of the time of this writing, no in-pile experiments have been performed, but now that the required devices have been developed to establish the feasibility of such an experiment, the germanium, quartz, stannous-oxide film wafer will be installed in the center of the core of the MIT Reactor in the liquid helium channel for the actual high flux neutron experiment.

LIST OF REFERENCES

1. Damask, A. C., and Dienes, G. J., Journal of Applied Physics , 29, 1713 (1958).

2. Brinkman, J. A., and Wiedersich, H., The Flow and Fracture of Materials in Nuclear Environments, STP 380, American Society for Testing and Materials, (1965) p.3.

3. Hesketh, R. V., Philosophical Magazine, 92, 1321 (1963).

4. Ross-Ross, P. A., Transactions of the American Nuclear Society, 10, 114 (1967).

5. Lewis, W. B., AECL-3251, (1969)

6. Glasstone, S., The Effects of Nuclear Weapons, (USAEC:1962), pp. 387-392.

7. Ziebold, T. O., Barnett, E. J., and Berte, F. J., MIT Reactor Cryogenic Facilities, Preliminary Design Report, (March 1968).

8. Kingery, W. D., Introduction to Ceramics, (New York: Wiley, 1963) p.498.

9. Kingery, W. D., Introduction to Ceramics, (New York: Wiley, 1963) p.468.

10. Bowman, H. F., "Influence of Nuclear Radiation on Pool-Boiling Heat Transfer to Liquid Helium", PhD. Thesis, MIT (1968).